iScience

CellPress
OPEN ACCESS

Article

DNA repair enzyme NEIL3 enables a stable neural representation of space by shaping transcription in hippocampal neurons

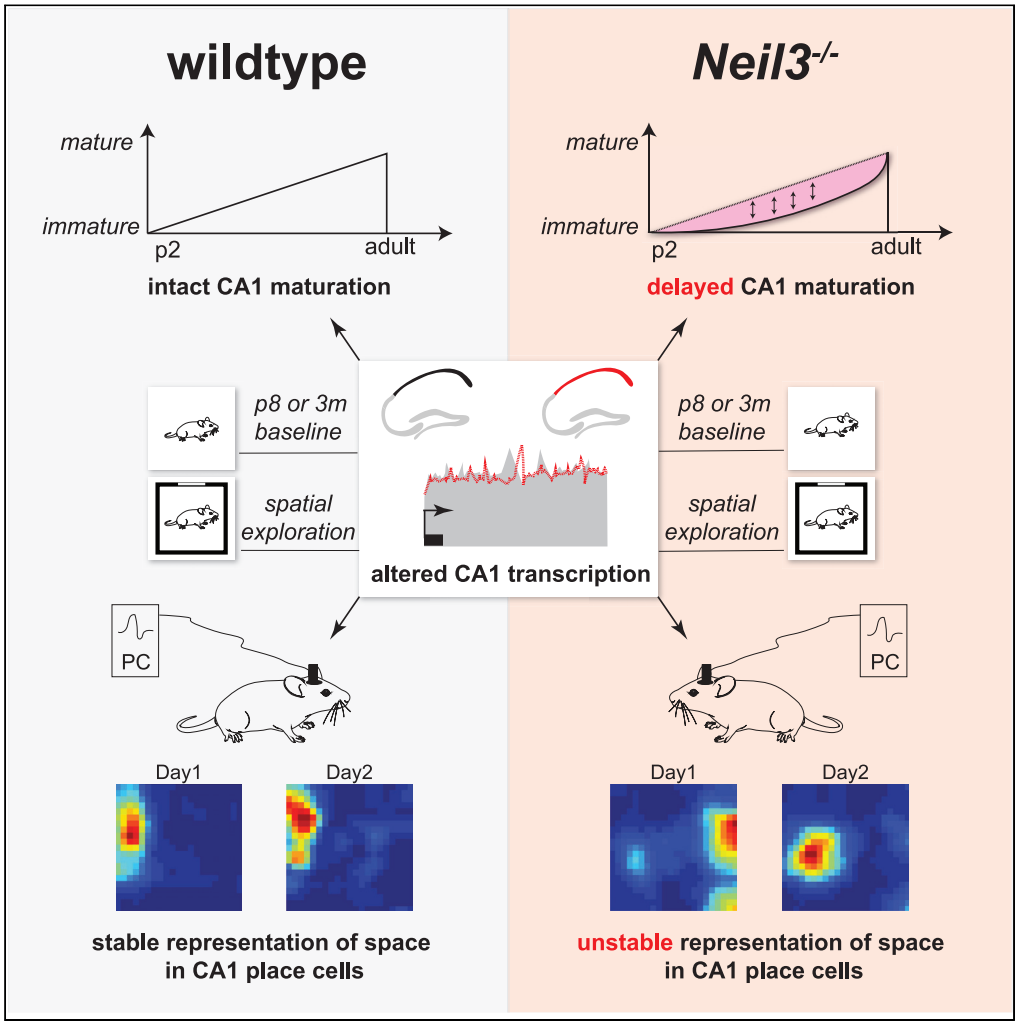

Nicolas Kunath, Anna Maria Bugaj, Pegah Bigonah, Marion Silvana Fernandez-Berrocal, Magnar Bjørås, Jing Ye

magnar.bjoras@ntnu.no (M.B.)
jing.ye@ntnu.no (J.Y.)

Highlights

NEIL3 impacts CA1 maturation by shaping transcription during development

NEIL3 depletion leads to impaired function of CA1 place cells

NEIL3 shapes transcription in hippocampal CA1 during behavior

NEIL3 impacts experience-induced expression of immediate early genes (IEGs).

Kunath et al., iScience 24, 103470
December 17, 2021
https://doi.org/10.1016/j.isci.2021.103470

iScience

CellPress
OPEN ACCESS

Article

DNA repair enzyme NEIL3 enables a stable neural representation of space by shaping transcription in hippocampal neurons

Nicolas Kunath,[1] Anna Maria Bugaj,[1] Pegah Bigonah,[1] Marion Silvana Fernandez-Berrocal,[1] Magnar Bjørås,[1,2,*] and Jing Ye[1,3,*]

SUMMARY

DNA repair enzymes are essential for the maintenance of the neuronal genome and thereby proper brain functions. Emerging evidence links DNA repair to epigenetic gene regulation; however, its contribution to different transcriptional programs required for neuronal functions remains elusive. In this study, we identified a role of the DNA repair enzyme NEIL3 in modulating the maturation and function of hippocampal CA1 neurons by shaping the CA1 transcriptome during postnatal development and in association with spatial behavior. We observed a delayed maturation in *Neil3*$^{-/-}$ CA1 and identified differentially regulated genes required for hippocampal development. We revealed impaired spatial stability in *Neil3*$^{-/-}$ CA1 place cells and found spatial experience-induced gene expression essential for synaptic plasticity. This is the first study that links molecular underpinnings of DNA repair to the neural basis of spatial cognition beyond animals' behavioral phenotypes, thus shedding light on the molecular determinants enabling a stable neural representation of space.

INTRODUCTION

Owing to the high oxidative load and free radicals produced by cellular metabolism in the brain, repair of oxidative DNA damages in neurons is extremely important for the maintenance of proper brain functions (Pan et al., 2014). Base excision repair (BER) is the major pathway for the removal of oxidized DNA bases (Krokan and Bjoras, 2013) and is known to play an essential role in active DNA demethylation (Wu and Zhang, 2017). The NEIL3 DNA glycosylase is one of the important enzymes initiating BER and has been implicated in diverse brain functions (Scheffler et al., 2019). NEIL3 is identified as a potential reader of oxidized methylcytosine (mC) derivatives (Spruijt et al., 2013) and is suggested to reactivate epigenetically silenced genes by an alternative BER pathway for DNA demethylation (Muller et al., 2014). Genome-wide alterations in the DNA epigenome and RNA transcriptome have been reported in the NEIL3-depleted heart (Olsen et al., 2017), suggesting a role of NEIL3-mediated BER in gene regulation. In the rodent brain, NEIL3 displays discrete expression patterns with enrichment in neurogenic niches such as the hippocampus and subventricular zone (Rolseth et al., 2008) and it has been shown to play a crucial role in induced and continuous adult neurogenesis (Sejersted et al., 2011; Regnell et al., 2012). Mice lacking NEIL3 have a normal lifespan without a predisposition to cancer or increased spontaneous mutation frequencies (Rolseth et al., 2017). However, *Neil3*$^{-/-}$ mice display an impaired spatial performance in the Morris Water Maze and a differential synaptic composition in the hippocampus (Regnell et al., 2012), suggesting a distinct role of NEIL3 in regulating hippocampal functions.

The hippocampus is the central hub for the encoding and recall of spatial and nonspatial episodic memories, in which heterogeneous representations of memory have been described. Place cells that encode spatial information in their firing patterns (place maps) are identified in all hippocampal subregions (O'Keefe and Dostrovsky, 1971; O'Keefe, 1979; Jung and McNaughton, 1993), and the association of place cell activity with spatial cognition has been demonstrated to support the cognitive map theory (Best et al., 2001). Recently, activity-dependent gene transcription has been defined to promote the plasticity of hippocampal circuits for cognition and behavior (Yap and Greenberg, 2018). Expression of specific immediate-early-gene tags hippocampal neurons as traces of context-dependent memory supporting the memory index theory (Goode et al., 2020). Further, a high degree of molecular heterogeneity has

[1]Department of Clinical and Molecular Medicine (IKOM), Norwegian University of Science and Technology (NTNU), 7034 Trondheim, Norway

[2]Department of Microbiology, Oslo University Hospital and University of Oslo, 0424 Oslo, Norway

[3]Lead contact

*Correspondence: magnar.bjoras@ntnu.no (M.B.), jing.ye@ntnu.no (J.Y.)

https://doi.org/10.1016/j.isci.2021.103470

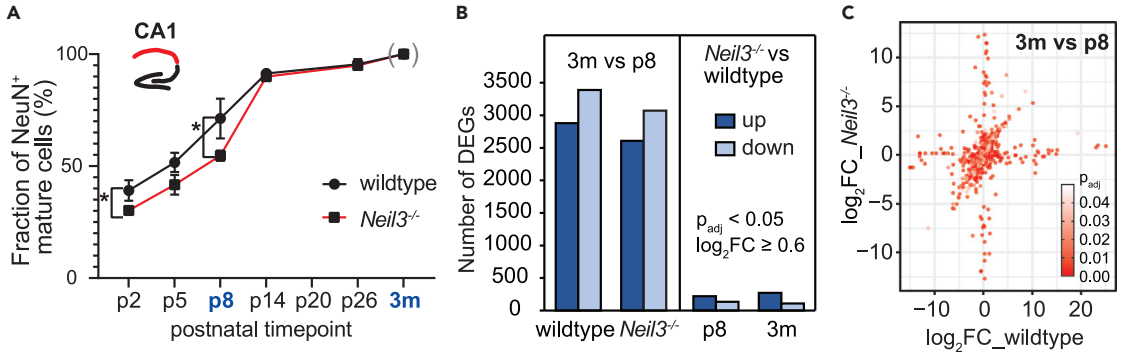
A
CA1
Fraction of NeuN+ mature cells (%)
100
50
0
wildtype
Neil3-/-
p2 p5 p8 p14 p20 p26 3m
postnatal timepoint
B
3m vs p8
Neil3-/- vs wildtype
up
down
Number of DEGs
3500
3000
2500
2000
1500
1000
500
0
padj < 0.05
log2FC ≥ 0.6
wildtype Neil3-/-
p8
3m
C
3m vs p8
log2FC_Neil3-/-
10
5
0
−5
−10
padj
0.04
0.03
0.02
0.01
0.00
−10 0 10 20
log2FC_wildtype

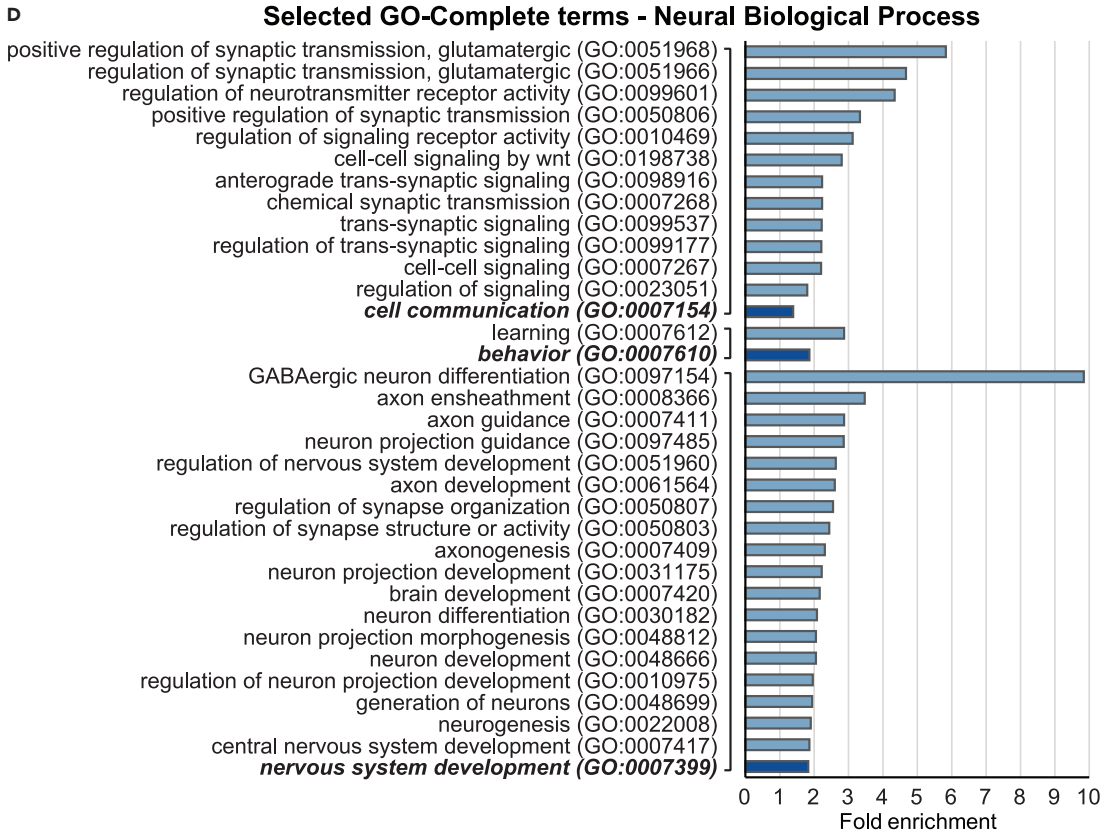
D
Selected GO-Complete terms - Neural Biological Process
positive regulation of synaptic transmission, glutamatergic (GO:0051968)
regulation of synaptic transmission, glutamatergic (GO:0051966)
regulation of neurotransmitter receptor activity (GO:0099601)
positive regulation of synaptic transmission (GO:0050806)
regulation of signaling receptor activity (GO:0010469)
cell-cell signaling by wnt (GO:0198738)
anterograde trans-synaptic signaling (GO:0098916)
chemical synaptic transmission (GO:0007268)
trans-synaptic signaling (GO:0099537)
regulation of trans-synaptic signaling (GO:0099177)
cell-cell signaling (GO:0007267)
regulation of signaling (GO:0023051)
cell communication (GO:0007154)
learning (GO:0007612)
behavior (GO:0007610)
GABAergic neuron differentiation (GO:0097154)
axon ensheathment (GO:0008366)
axon guidance (GO:0007411)
neuron projection guidance (GO:0097485)
regulation of nervous system development (GO:0051960)
axon development (GO:0061564)
regulation of synapse organization (GO:0050807)
regulation of synapse structure or activity (GO:0050803)
axonogenesis (GO:0007409)
neuron projection development (GO:0031175)
brain development (GO:0007420)
neuron differentiation (GO:0030182)
neuron projection morphogenesis (GO:0048812)
neuron development (GO:0048666)
regulation of neuron projection development (GO:0010975)
generation of neurons (GO:0048699)
neurogenesis (GO:0022008)
central nervous system development (GO:0007417)
nervous system development (GO:0007399)
0 1 2 3 4 5 6 7 8 9 10
Fold enrichment

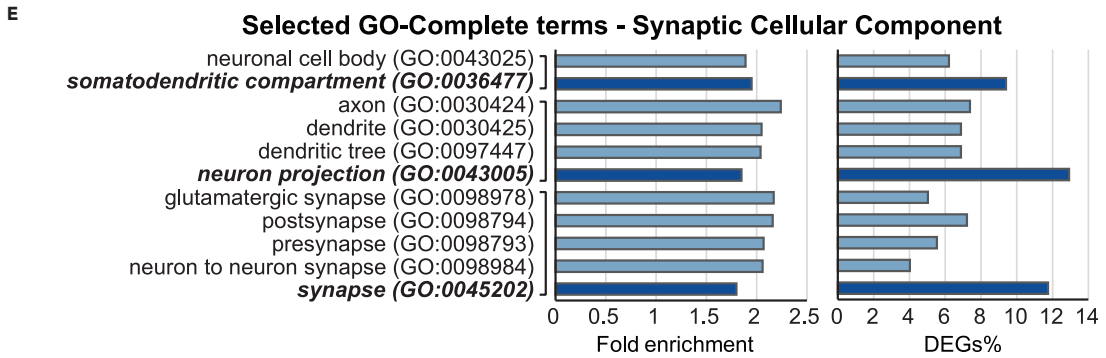
E
Selected GO-Complete terms - Synaptic Cellular Component
neuronal cell body (GO:0043025)
somatodendritic compartment (GO:0036477)
axon (GO:0030424)
dendrite (GO:0030425)
dendritic tree (GO:0097447)
neuron projection (GO:0043005)
glutamatergic synapse (GO:0098978)
postsynapse (GO:0098794)
presynapse (GO:0098793)
neuron to neuron synapse (GO:0098984)
synapse (GO:0045202)
0 0.5 1 1.5 2 2.5
Fold enrichment
0 2 4 6 8 10 12 14
DEGs%

Figure 1. NEIL3 impacts CA1 maturation by shaping neuronal transcriptome

(A) The fraction of CA1 mature neurons with high NeuN immunofluorescent intensity was analyzed during the first postnatal month and at adulthood (n = 6 wild type and *Neil3*$^{-/-}$ mice per time points, mean ± SEM, p < 0.05, two-way-ANOVA/Sidak's). P8 and 3 m samples were further explored in the transcriptome and therefore highlighted.

(B) Bar-diagrams show numbers of differentially expressed genes (DEGs, $p_{adj} < 0.05$ and ABS ($log_2FC \geq 0.6$)) in wildtype and *Neil3*$^{-/-}$ CA1 across ages (left, 3 m vs p8) as well as in p8-immature and adult-mature (3 m) CA1 across genotypes (*Neil3*$^{-/-}$ vs wild type). The number of animals used for the transcriptome analysis was n = 4 per genotype at p8, n = 3 per genotype at 3 m.

(C) The interaction plot represents the 1799 genes that had statistically different ($p_{adj} < 0.05$, color-coded) patterns of expression across ages (3 m vs p8) in wild type and *Neil3*$^{-/-}$ CA1. The log_2(Fold Change) of DEGs in wild type and *Neil3*$^{-/-}$ CA1 was shown on the x-axis and y- axis, respectively. The effect size of interaction is represented by the position of dots representing genes (distance from the diagonal).

(D) Selected GO-Complete Biological Process (BP) terms related to neuronal functions (FDR<0.05, full list in Table S2).

(E) Selected GO-Complete Cellular Component (CC) terms related to synaptic functions (FDR<0.05, full list in Table S1). The dark bars represent the ancestral terms, and the light bars represent the child terms.

been delineated in the hippocampal formation, which is spatially patterned and associated with anatomical, physiological, and functional varieties of hippocampal neurons (Cembrowski and Spruston, 2019). However, the molecular mechanisms governing the function of specialized hippocampal cell types are far less understood.

In this study, we elucidated a novel function of NEIL3 in hippocampal CA1 pyramidal cells at both molecular and functional levels. We observed a delayed CA1 maturation in *Neil3*$^{-/-}$ mice and revealed distinct changes in the CA1 transcriptome across postnatal development, implicating a role of NEIL3-dependent gene modulation in the structural and functional development of the hippocampus. We studied functional properties of *Neil3*$^{-/-}$ CA1 place cells and detected impaired long-term spatial stability, demonstrating a functional interference of NEIL3 in hippocampal neurons. We identified spatial experience-induced gene expression in *Neil3*$^{-/-}$ CA1 cells, suggesting NEIL3-dependent modulation of gene expression in synaptic plasticity during behavior. We found experience-induced expression of immediate early genes, implicating a role of NEIL3 in the molecular correlates of memory engrams. Our work provides evidence that NEIL3 shapes the CA1 transcriptome during development and behavior, which is essential for the functional plasticity of hippocampal CA1 neurons.

RESULTS

NEIL3 impacts CA1 maturation by shaping the neuronal transcriptome

NEIL3 is expressed in the developing central nervous system with high expression in early postnatal days (Rolseth et al., 2008). Depletion of NEIL3 did not affect brain size in relation to body weight in mice (Figure S1A). We questioned whether NEIL3 was important for the postnatal maturation of hippocampal neurons. From postnatal day 2 (p2) up to an adult age (3 months), we monitored the maturation of hippocampal CA1 neurons by immunohistochemistry (IHC) using the neuronal marker NeuN. The intensity of NeuN immunoreactivity is high in mature hippocampal neurons, but weak in immature ones that is often associated with the expression of doublecortin (DCX) and beta III tubulin (Tubb3) (Figures S1B–S1E) (von Bohlen Und Halbach, 2007). The fraction of strong NeuN^{+} mature neurons increased sharply from p2 to p14 in both wild type and *Neil3*$^{-/-}$ CA1 (Figures 1A and S1D). Significantly, a reduced fraction of NeuN^{+} mature neurons was detected in *Neil3*$^{-/-}$ CA1 compared to the wild type at p2 (wt 39% vs *Neil3*$^{-/-}$ 30%, p = 0.0412) and p8 (wt 71% vs *Neil3*$^{-/-}$ 55%, p = 0.0210, two-way-ANOVA/Sidak's), suggesting a delayed CA1 maturation in *Neil3*$^{-/-}$ mice.

Then we examined the transcriptome of p8 and adult (3 m) CA1 in wild type and *Neil3*$^{-/-}$ mice. Whole-transcriptome sequencing (RNAseq) was performed using RNA samples from micro-dissected dorsal CA1 by a needle-scratch-approach (see STAR Methods). Differential gene expression was analyzed using DESeq2 (Love et al., 2014). To assess the impact of NEIL3 on CA1 transcriptome across postnatal development, we performed multifactorial analysis by adding interaction of age and genotype (the differential gene expression by a synergy of both factors, see STAR Methods). As expected, the expression level of NEIL3 was high in p8, low in adult CA1 of wild type mice (3 m vs p8, log2FC = −3.16, padj <0.0001), and not detected in the knockout samples (Figures S3A and S3B). In both wild type and *Neil3*$^{-/-}$ CA1, the expression of immature neuronal markers such as DCX and beta III tubulin (Tubb3) was high in p8 but low in 3 m of CA1 samples, whereas both NeuN and Wfs1 (markers of mature neurons) were highly expressed in 3 m compared to the p8 samples (Figure S3C). No significant difference was observed between the genotypes

(*Neil3*$^{-/-}$ vs wild type) at the bulk RNA level. This result supports that most CA1 neurons are still immature at p8 and continue developing postnatally.

We identified thousands of genes that were either significantly upregulated or downregulated ($p_{adj} < 0.05$) across the CA1 development (3 m vs p8) or between the genotypes (*Neil3*$^{-/-}$ vs wild type) (Figure S3D). The ones that passed the criterion of ABS (log_2FC) ≥ 0.6 [ABS (fold change) > 1.5] were defined as differentially expressed genes (DEGs). As expected, a large number of DEGs across the CA1 development (3 m vs p8) were identified in wild type (6269 genes with 2880 upregulated and 3389 downregulated) as well as in *Neil3*$^{-/-}$ mice (5679 genes with 2608 up- and 3071 down-regulated) (Figure 1B, left panel), supporting distinct transcriptional programs in immature and mature CA1 across development. Further, comparison of wild type and *Neil3*$^{-/-}$ CA1 revealed several hundreds of NEIL3-specific DEGs at p8 (352 genes with 219 up- and 133 down-regulated) and at adulthood (382 genes with 272 up- and 110 down-regulated) (Figure 1B, right panel), suggesting a role of NEIL3 in shaping the CA1 transcriptome. The interaction analysis discovered 1799 genes that had statistically different ($p_{adj} < 0.05$) patterns of expression in *Neil3*$^{-/-}$ CA1 compared to the wild type in the trajectory of development (from the immature p8 to the fully matured 3 m adult stage) (Figures 1C and S3E). Of those genes, 605 passed the threshold of ABS (difference in log_2 Fold Change) ≥ 0.6, therefore considered as the DEGs of particular importance for understanding the delayed CA1 maturation in mice lacking NEIL3.

NEIL3 impacts development-associated gene expression essential for the structure and functional development of hippocampal CA1

By using the Gene Ontology (GO) consortium/PANTHER classification system (Mi et al., 2019), the 605 of NEIL3-specific development-associated DEGs were analyzed for the attributed cellular components (CC) and biological processes (BP) (Tables S1 and S2). These DEGs were involved in a broad spectrum of neural biological processes, including parent terms "nervous system development (GO:0007399)," "cell communication (GO:0007154)," "behavior (GO: 0007610) and their respective sub-terms (Figure 1D), demonstrating an importance of NEIL3-dependent DEGs for hippocampal development and functions. In addition, some of the DEGs were highly attributed to the cellular components essential for synaptic functions. The overrepresented GO-CC terms included "synapse (GO:0045202, 70 out of 605 DEGs)", "neuron projection (GO:0043005, 77 out of 605 DEGs)" and "somatodendritic compartment (GO:0036477, 56 out of 605 DEGs)" (Figure 1E). A total of 98 genes were extracted after merging the DEGs enriched in any of the three GO-CC terms. We defined them as a group of "Synaptic-CC DEGs", which showed different expression patterns across ages (3 m vs p8) and genotypes (*Neil3*$^{-/-}$ vs wild type) (Figure 2A).

Among the 98 "Synaptic-CC DEGs" in *Neil3*$^{-/-}$ CA1, 47 genes were found to be differentially regulated at p8 and 64 genes at 3 m (13 overlapping DEGs in both age groups). The top 30 ones were different at p8 and 3 m except for *Gabra2* that was downregulated in both age groups (Figures 2B and 2C). These DEGs were overrepresented in distinct biological processes in immature and mature CA1 neurons. At p8 (immature CA1), genes (e.g., *Cldn11*, *Mbp*, *Mag*, and *Mtmr2*) involved in "axon ensheathment (GO:0008366)" as well as the ones (e.g., *Micall2*, *Nrp2*, *Smo*, and *Thbs4*) in "neuron projection development (GO:0031175)" were highly upregulated, whereas genes (e.g., *Grid2*, *Gabra2*, *Ptprf*, *Ntrk1*) involved in "synapse organization (GO:0050808)" and/or "regulation of synapse organization (GO:0050807)" were downregulated in *Neil3*$^{-/-}$ CA1 (Figure 2D), all of which may contribute to a delay of CA1 maturation. In adult CA1 (mature state), the most differentially regulated genes in *Neil3*$^{-/-}$ mice (e.g., *Pdyn*, *Drd2*, *Adcyap1*, *Th*, *Gabra2*, *Kdr*, *Tac1*, *Cacng4*, *Chrm4*, *Grm2*, *Rph3a*, and *Rims1*) were overrepresented in "synaptic signaling (GO:0099536)" and/or "regulation of trans-synaptic signaling (GO:0099177)" and/or other related BP-terms (Figure 2E), supporting a functional relevance of NEIL3 for regulation of synaptic processes. In addition, some of the "Synaptic-CC DEGs" in *Neil3*$^{-/-}$ adult CA1 were engaged in specific pathways (PANTHER), such as "Dopamine receptor mediated signaling pathway (P05912)", "Metabotropic glutamate receptor group II pathway (P00040)" and "Heterotrimeric G-protein alpha signaling pathway (P00026/P00027)", implying a potential role of NEIL3 in molecular mechanisms regulating synaptic signaling events in mature CA1 neurons. This result suggests that NEIL3-dependent gene modulation is involved in the structural and functional development of the hippocampus, which is crucial for the hippocampal dependent cognitive function in adults.

Neil3$^{-/-}$ CA1 place cells displayed normal spatial activity

Next, we assessed whether *Neil3*$^{-/-}$ CA1 neurons were functional normal. It is well-known that hippocampal place cells encode spatial information in their environment-specific firing patterns ("place fields")

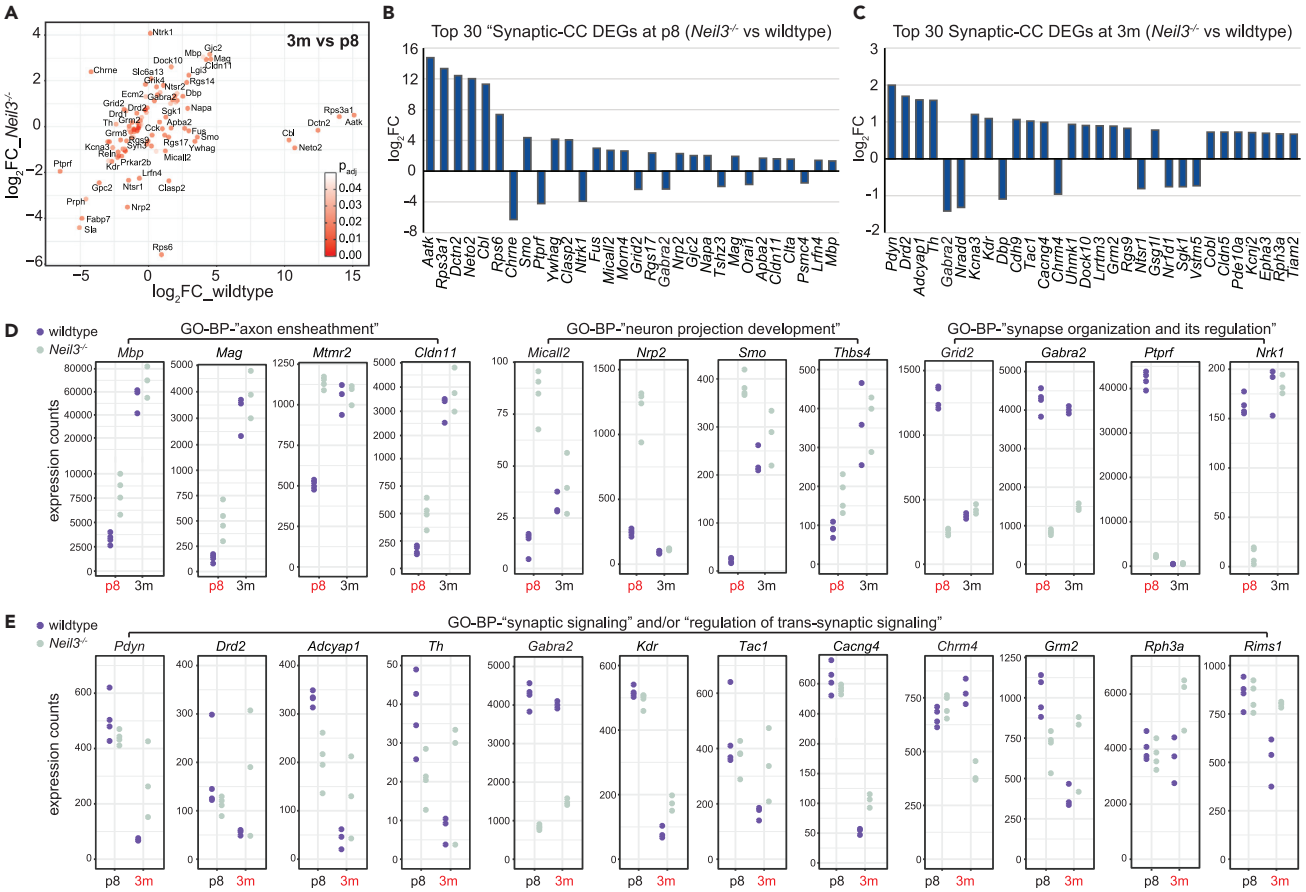

Figure 2. NEIL3-specific and development associated DEGs essential for synaptic functions

(A) The interaction plot represents the selected "Synaptic-CC DEGs (98 genes)" in *Neil3*$^{-/-}$ CA1 that had different expression patterns (p_{adj} < 0.05, color-coded) across ages (3 m vs p8) in wild type and *Neil3*$^{-/-}$ CA1. The log_2FC (Fold Change) of DEGs in wild type and *Neil3*$^{-/-}$ CA1 is shown on the x-axis and y-axis, respectively. The effect size of interaction is represented by position of dots representing genes (distance from the diagonal).

(B) The bar-plot represents the top 30 NEIL3-dependent "Synaptic-CC DEGs" in p8 CA1.

(C) The bar-plot represents the top 30 NEIL3-dependent "Synaptic-CC DEGs" in adult CA1.

(D) The selected DEGs associated with biological processes such as "axon ensheathment", "neuron projection development", "synapse organization and regulation" are listed. Differential regulation is more pronounced in immature p8-CA1 of *Neil3*$^{-/-}$ mice.

(E) The selected DEGs associated with the biological processes of synaptic signaling and regulation are listed. Differential regulation is more pronounced in mature CA1 of *Neil3*$^{-/-}$ mice (3 m). Dot-plots represent normalized counts of individual animals at p8 (4x wild type and 4x *Neil3*$^{-/-}$ mice) and at 3 m (3x wild type and 3x *Neil3*$^{-/-}$ mice).

(O'Keefe and Dostrovsky, 1971). We recorded CA1 place cell activity in adult mice (3–6 m) while the animals were freely moving in an open field environment (Figures 3A and 3B). The implant locations were evenly distributed along the proximodistal axis of CA1 in both genotypes (Figure 3C), as space is represented non-uniformly along the transverse axis of CA1 (Henriksen et al., 2010). Place cells were defined as cells with scores for spatial information content passing the 95th percentile of a distribution for randomly shuffled data from all recorded CA1 cells within the group (Figure 3D, spatial information content above 0.554 for wild type and above 0.547 for *Neil3*$^{-/-}$). Based on this criterion, we identified a total of 355 place cells (85% of 419 putative principal neurons recorded) in wild type (n = 4) and 313 place cells (78% of 402 putative principal neurons recorded) in *Neil3*$^{-/-}$ (n = 4) mice. Most CA1 place cells had a single environment-specific firing pattern (the "place field"), but more than one place field was also observed in some cases (Figure 3B and S3). A higher fraction of place cells in *Neil3*$^{-/-}$ CA1 displayed multiple firing fields (29% vs 18% in wild type, Figures 3E and 3F). The average number of place fields differed significantly (wt: 1.22 ± 0.03, *Neil3*$^{-/-}$: 1.39 ± 0.04 [mean ± SEM], p = 0.0001 unpaired t-test with Welch's correction and $p_{corr.}$ = 0.0441 nested t-test). We also assessed a range of electrophysiological characteristics for all place cells in the wild type and *Neil3*$^{-/-}$ groups (Figure 3E). No difference was observed regarding spatial information

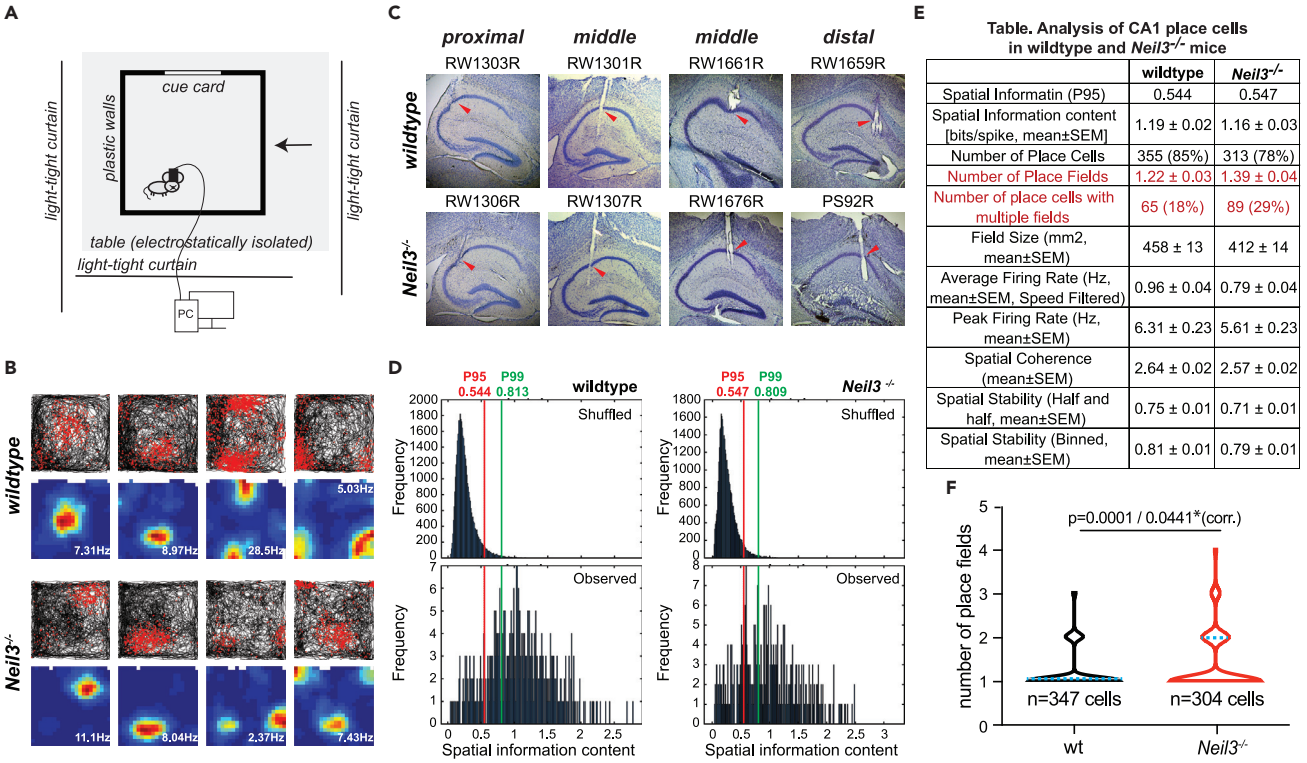

	wildtype	Neil3-/-
Spatial Informatin (P95)	0.544	0.547
Spatial Information content [bits/spike, mean±SEM]	1.19 ± 0.02	1.16 ± 0.03
Number of Place Cells	355 (85%)	313 (78%)
Number of Place Fields	1.22 ± 0.03	1.39 ± 0.04
Number of place cells with multiple fields	65 (18%)	89 (29%)
Field Size (mm2, mean±SEM)	458 ± 13	412 ± 14
Average Firing Rate (Hz, mean±SEM, Speed Filtered)	0.96 ± 0.04	0.79 ± 0.04
Peak Firing Rate (Hz, mean±SEM)	6.31 ± 0.23	5.61 ± 0.23
Spatial Coherence (mean±SEM)	2.64 ± 0.02	2.57 ± 0.02
Spatial Stability (Half and half, mean±SEM)	0.75 ± 0.01	0.71 ± 0.01
Spatial Stability (Binned, mean±SEM)	0.81 ± 0.01	0.79 ± 0.01

Figure 3. CA1 place cells recorded in wild type and *Neil3*$^{-/-}$ mice

(A) Schematic illustration of the experimental set-up for extracellular neuronal live recordings.

(B) Firing pattern of representative place cells recorded in wild type and *Neil3*$^{-/-}$ CA1. Trajectory maps with superimposed spike locations (red dots) are shown at top and color-coded rate maps (red for peak and blue for firing rates) with indicated peak firing rate are shown at bottom.

(C) Cresyl-violet-stained hippocampal sections showing the tetrode locations (pointed by red arrows) in all implanted animals (n = 4 wild type and n = 4 *Neil3*$^{-/-}$ mice).

(D) Distributions of observed spatial information scores and the randomly shuffled data for the entire cell samples recorded in wild type or *Neil3*$^{-/-}$ CA1. The 95th and the 99th percentile of the shuffled distribution are marked by the red and green line. The 95th percentile was used as a threshold to define place cells.

(E) Table of general electrophysiological properties of place cells in wild type versus *Neil3*$^{-/-}$ mice. Data were represented as mean ± SEM. Significant differences were observed in *Neil3*$^{-/-}$ CA1 regarding the number of place fields per cell and the fraction of place cells with multiple place fields, marked in red.

(F) Violin plot illustrating the number of place fields per place cell in wild type and *Neil3*$^{-/-}$ CA1(blue line indicates median). The average number of place fields differed significantly between genotypes ($p_{corr.}$ = 0.0441, nested t-test).

content (wt: 1.19 ± 0.02, *Neil3*$^{-/-}$: 1.16 ± 0.03, mean ± SEM across cells), spatial coherence (wt: 0.88 ± 0.02, *Neil3*$^{-/-}$: 0.88 ± 0.02) or within-session spatial stability (wt: 0.75 ± 0.01, *Neil3*$^{-/-}$: 0.71 ± 0.01). Minor differences were observed in the mean firing rate (wt: 0.96 ± 0.04Hz, *Neil3*$^{-/-}$: 0.79 ± 0.04Hz, p = 0.0012 and $p_{corr.}$ = 0.3645), peak firing rate (wt: 6.31 ± 0.23Hz, *Neil3*$^{-/-}$: 5.61 ± 0.23Hz, p = 0.0375 and $p_{corr.}$ = 0.5519) and mean field size (wt: 458 ± 13 mm^2, *Neil3*$^{-/-}$: 412 ± 014 mm^2, p = 0.0181 and $p_{corr.}$ = 0.3245) (Figure 3E). These observations demonstrate generally normal spatial activity of CA1 place cells in mice lacking NEIL3.

Neil3$^{-/-}$ CA1 place cells displayed impaired spatial stability

Hippocampal place cells are able to maintain a stable spatial map in the familiar environment and alter their firing patterns upon environmental changes (termed "remapping") (Muller and Kubie, 1987; Bostock et al., 1991). When animals are exposed to a novel environment, place fields of specific cells may change in firing rate, shift in location, appear or disappear, a process known as "global remapping" (Leutgeb et al., 2005). We recorded CA1 place cells in wild type and *Neil3*$^{-/-}$ mice over five sequential sessions in the familiar or novel environments consisting of a black or white colored square recording chamber (see STAR Methods and Figure 4A). Spatial global remapping was measured by cross-correlation of rate maps from the same cell recorded in two different environments (familiar vs novel). Both wild type and *Neil3*$^{-/-}$ place cells

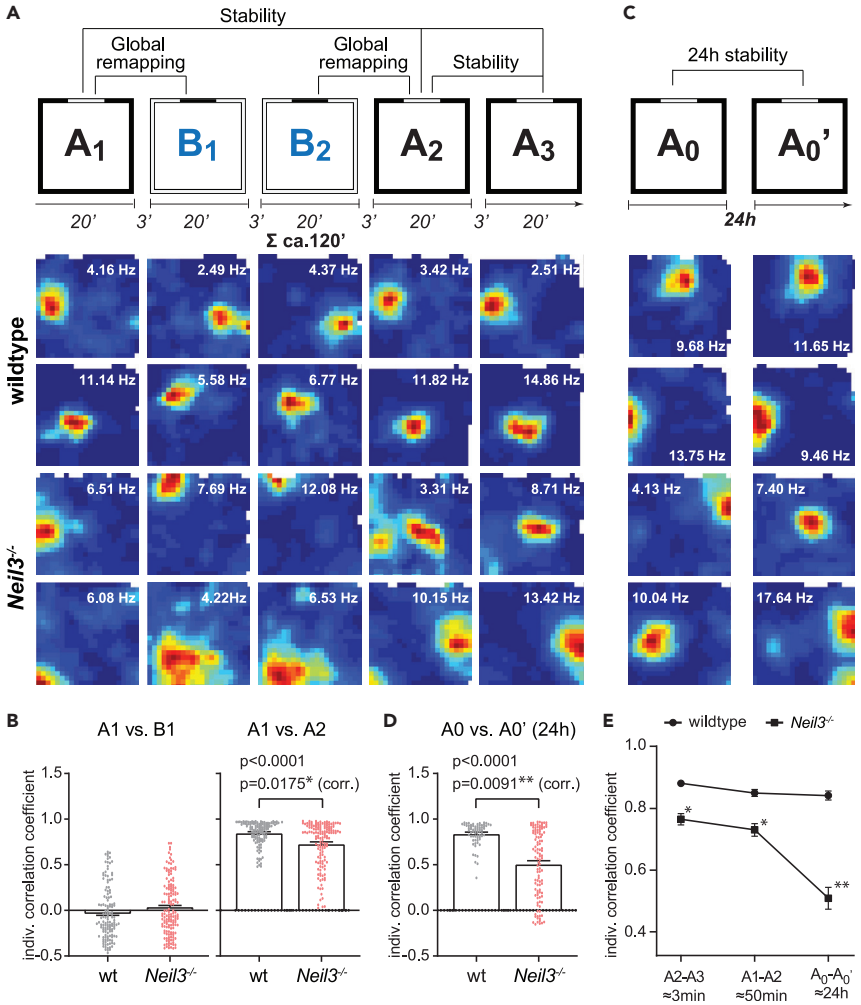

Figure 4. *Neil3*$^{-/-}$ CA1 place cells displayed impaired spatial stability

(A) CA1 place cells in wild type and *Neil3*$^{-/-}$ mice were recorded for five sessions (20 min of recording and 3 min of rest) in a sequence of familiar (Room A) and novel (Room B) environments (top row). Global remapping of place cells was observed in both genotypes from the familiar environment A (trial in A_1) to the novel environment B (trials in B_1 and B_2). Wildtype place cells widely retrieved original maps when re-exposed to the familiar environment (trials in A_2 and A_3), whereas a proportion of *Neil3*$^{-/-}$ place cells kept generating new maps. Rate maps of two representative place cells in wild type and *Neil3*$^{-/-}$ CA1 are shown, and peak firing rates are indicated.

(B) Correlation coefficients between trials in A_1 and B_1 or in A_1 and A_2 were analyzed for the whole population of wild type and *Neil3*$^{-/-}$ place cells.

(C) The firing patterns of place cells in the familiar environment A were re-tested after one day (A_0 and A_0', ca. 24-h interval, as illustrated). Wildtype place cells largely kept the same firing patterns in both trials, whereas *Neil3*$^{-/-}$ place cells often generated new maps in the second trial on Day 2. Rate maps of two representative place cells in wildtype and *Neil3*$^{-/-}$ CA1 are shown, and peak firing rates are indicated.

(D) Correlation coefficients between trials in A_0 and A_0' were analyzed for the whole population of wildtype and *Neil3*$^{-/-}$ place cells that were monitored over the course of 24 h.

(E) The line graph shows the deteriorated spatial correlation of *Neil3*$^{-/-}$ place cells in the familiar environments over a longer time course. Statistics were conducted using unpaired t-test with Welch's correction at the population level (each cell as statistical unit) and using a nested t-test at an animal level ($p_{corr.}$, each animal as statistical unit, n = 4 for each genotype). Data in histograms were represented as mean ± SEM.

reliably remapped to the new environment with similar low correlation coefficients in the whole population (A1 vs B1, wt −0.028 ± 0.026 vs *Neil3*$^{-/-}$ 0.030 ± 0.024 [mean ± SEM], $p > 0.1$, Figures 4A, 4B, and S5B), suggesting that NEIL3-dependent modulation of transcription and thereafter synaptic changes are not essential for the remapping of CA1 place cells.

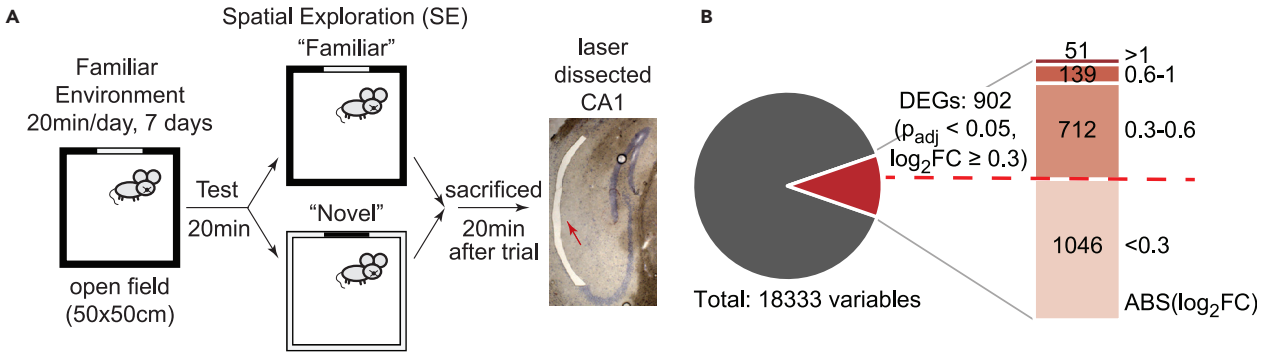

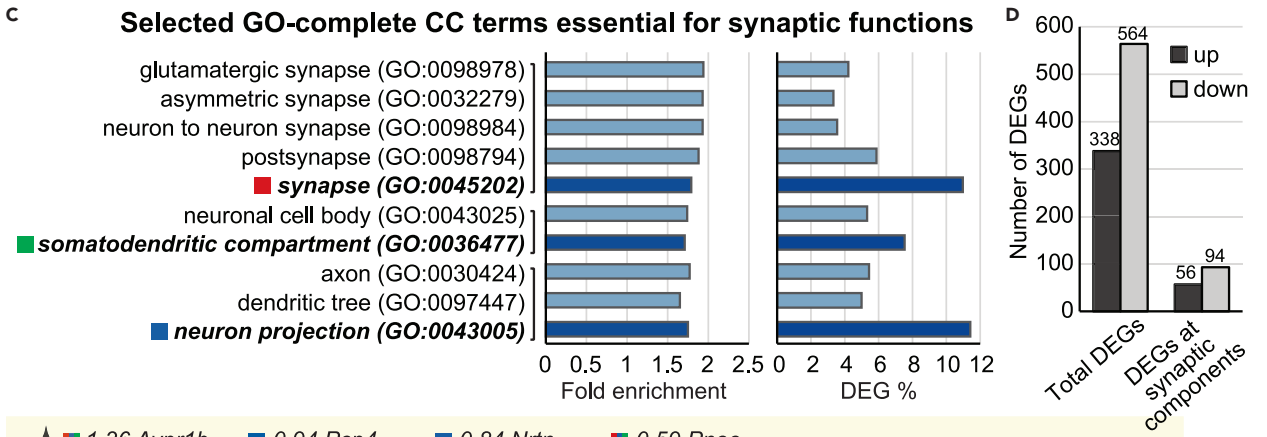

Up	1.36 Avpr1b	0.94 Pcp4	0.84 Nrtn	0.59 Pnoc	
	1.34 Ntf3	0.91 Htr7	0.60 Lamp5	0.59 Scrg1	
Down	-1.62 Gabra2	-1.17 Kcnk9	-0.83 Tenm1	-0.67 Cacna1g	-0.61 Slc17a6	-0.55 Cacna1e
	-1.50 Grm2	-1.09 Marcksl1	-0.80 Hap1	-0.65 Cit	-0.58 Robo3	-0.55 Trpm4
	-1.45 Pde11a	-0.98 Inha	-0.77 Sdk1	-0.64 Atp2b4	-0.57 Pcdh8	
	-1.22 Npbwr1	-0.90 Wnt3a	-0.68 Rgs9	-0.63 Ntsr1	-0.56 Prrt1	

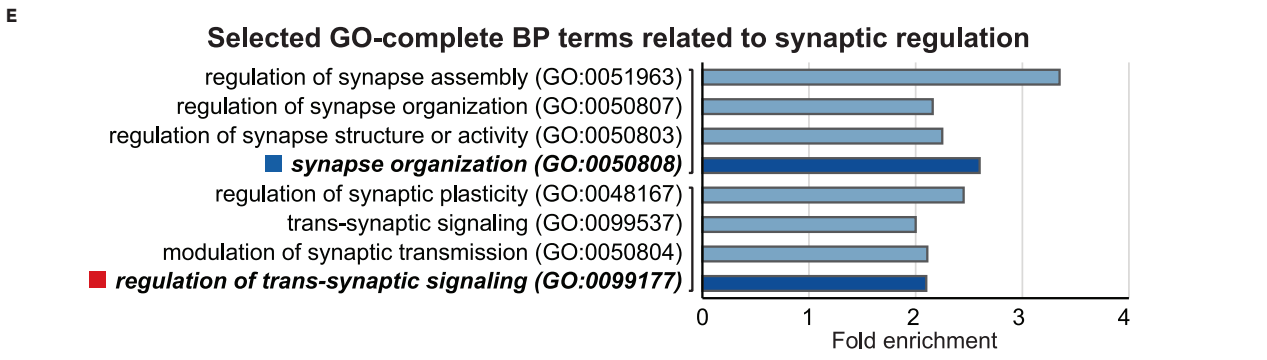

Up	1.34 Ntf3	0.66 Gfap	0.52 S100b	0.48 Fam107a	0.43 Car2
	0.91 Htr7	0.55 Itgam	0.50 Wnt7b	0.45 Tyrobp	0.42 Plcl1
Down	-1.62 Gabra2	-0.77 Sdk1	-0.56 Prrt1	-0.44 L1cam	-0.43 Slc6a6
	-1.50 Grm2	-0.63 Ntsr1	-0.48 Nos1	-0.44 Itga3	-0.42 Kmt2a
	-0.90 Wnt3a	-0.63 Col4a1	-0.46 Syngap1	-0.44 Kirrel3	-0.42 Grin2d
	-0.80 Hap1	-0.57 Pcdh8	-0.45 Grin2a	-0.44 Unc13b	-0.42 Lrrk2

Figure 5. Gene Ontology overrepresentation analysis of differentially expressed genes (DEGs) in *Neil3*$^{-/-}$ CA1 neurons after spatial exploration

(A) Schematic illustration of the experimental design. "Familiar" and "Novel" were combined as one spatial exploration (SE) condition with n = 5 for wildtype and n = 6 for *Neil3*$^{-/-}$.

(B) Pie chart showing the proportion of DEGs (Benjamini-Hochberg $p_{adj} < 0.05$) passing different thresholds of ABS (log_2FC). 902 DEGs passing the ABS ($log_2FC \geq 0.3$) (separated by the red-colored dotted line) were used in a Gene Ontology (GO) overrepresentation analysis.

(C) Selected GO-Complete Cellular Component (CC) terms (FDR<0.05, full list in Table S3). The dark bars represent the ancestral terms, and the light bars represent the child terms. Three ancestral terms (highlighted and color-coded), "synapse (red)", "neuron projection (blue)" and "somatodendritic compartment (green)", were defined as terms for synaptic components. The top 30 NEIL3-dependent DEGs (log_2FC values were indicated, marked with up or down-regulation) overrepresented in different synaptic cellular components (color-coded as shown above) are listed below.

(D) Bar-plot showing the proportion of up- and down-regulated DEGs in total and DEGs annotated with synaptic function related GO-CC terms.

(E) Selected GO-Complete Biological Process (BP) terms related to synaptic regulation (FDR<0.05, full list in Table S4). The dark bars represent the ancestral terms, and the light bars represent the child terms. The ancestral terms, "synapse organization" and "regulation of trans-synaptic signaling", are highlighted and color coded with blue and red. The top 30 NEIL3-dependent DEGs (log_2FC values are indicated and marked with up- or down-regulation) overrepresented in respective BP terms (color-coded as shown above) are listed below.

Further, we assessed spatial stability by comparing rate maps from the same cell recorded in the same familiar environment A but at different sessions. 2.3% of place cells in the wild type, but 18.5% in *Neil3*$^{-/-}$ CA1, expressed correlation coefficients lower than 0.5 across two familiar environments (A1 vs A2, 50-min interval). The mean correlation coefficient was significantly lower in the population of *Neil3*$^{-/-}$ place cells (wt 0.851 $\pm$ 0.011 vs *Neil3*$^{-/-}$ 0.731 $\pm$ 0.020 [mean $\pm$ SEM], $p < 0.0001$ and $p_{corr.} = 0.0175$), indicating that a larger fraction of *Neil3*$^{-/-}$ place cells had shifted place maps in the familiar environment after two novel environment trials (Figures 4A, 4B, and S5C). Lower spatial correlation was also observed in *Neil3*$^{-/-}$ place cells recorded in two sequential sessions (A2 vs A3, ca. 3-min interval) with 14.8% of cells having correlation coefficients below 0.5 (0% of wild type cells, Figure S5C, wt 0.882 $\pm$ 0.011 vs *Neil3*$^{-/-}$ 0.765 $\pm$ 0.018 [mean $\pm$ SEM], $p < 0.0001$ and $p_{corr.} = 0.0235$). These results suggest impaired spatial stability in CA1 place cells lacking NEIL3.

To further assess the long-term spatial stability of *Neil3*$^{-/-}$ place cells, we monitored the firing patterns (place maps) of place cells in the same familiar environment for two days with a 24-h interval. We reliably recorded 68 wild type and 113 *Neil3*$^{-/-}$ place cells over two days (all cells listed in Data S1). A further increased fraction of *Neil3*$^{-/-}$ place cells (44.4%) did not retrieve the original place maps in the same environment recorded on day 2 (1.5% of wild type cells, correlation coefficients below 0.5) with a significantly lower correlation coefficient in the whole population (Figures 4C and 4D, wt 0.842 $\pm$ 0.015 vs *Neil3*$^{-/-}$ 0.509 $\pm$ 0.036 [mean $\pm$ SEM], $p < 0.0001$ and $p_{corr.} = 0.009$). The spatial correlation of *Neil3*$^{-/-}$ place cells in the familiar environments was remarkably deteriorated when cells were recorded over a longer time course (Figures 4E and S5D, 0.765 $\pm$ 0.018 [A2 vs A3, ca.3 min], 0.731 $\pm$ 0.020 [A1 vs A2, ca.50 min], 0.509 $\pm$ 0.036 [24 h], $p < 0.0001$ for both A1A2 vs. A0A0′ and A2A3 vs. A0A0′, mixed model, Sidak's multiple comparisons test). These results demonstrated that *Neil3*$^{-/-}$ place cells displayed impaired long-term spatial stability, linking to the decreased spatial performance observed in *Neil3*$^{-/-}$ mice (Regnell et al., 2012).

NEIL3 impacts spatial experience-induced gene expression associated with synaptic regulation

Experience-induced transcription has been demonstrated in hippocampal neurons that are critical for learning and memory (Eagle et al., 2016). As NEIL3 was detected in wild type adult CA1 (Figures S3A and S3B), we questioned whether NEIL3 had a direct impact on the spatial experience dependent gene expression. Wild type and *Neil3*$^{-/-}$ mice were exposed to a spatial exploration paradigm (Figure 5A and see method), in which the sequence from a familiar to a novel environment was identical to the one used to induce global remapping of CA1 place cells as shown in Figure 4. To increase the purity of CA1-pyramidal samples, we precisely isolated the dorsal CA1 pyramidal layer by laser capture microdissection (LCM). Similar RNAseq was performed, and differential gene expression was analyzed with DESeq2. As no differential gene expression was detected in the wild type or the *Neil3*$^{-/-}$ group after novel environment stimuli (all genes had a $P_{adj} \approx 1$ with DESeq2), we merged samples to one "spatial exploration" (SE) condition and analyzed differential gene expression in *Neil3*$^{-/-}$ CA1 after spatial exploration. In this case, a total of 1948 genes had statistically differential expression ($P_{adj} < 0.05$), including 190 genes that passed ABS (log_2FC) $\geq$0.6 and 902 genes that passed ABS (log_2FC) $\geq$0.3 (Figure 5B). To include all possible NEIL3-dependent genes that are potentially biologically relevant, genes that passed a threshold of ABS (log_2FC) $\geq$ 0.3 were defined as experience-induced DEGs in *Neil3*$^{-/-}$ CA1. Within this body of differentially

regulated genes, 37% (338 out of 902 DEGs) were upregulated and 63% (564 out of DEGs) were downregulated. Meanwhile, differential gene expression in the baseline condition (no behavioral intervention) of *Neil3*$^{-/-}$ CA1 (laser-dissected samples) was analyzed as a reference (Figure S6).

NEIL3-associated DEGs after spatial exploration were again highly overrepresented in cellular components essential for synaptic functions, including the GO-CC parent terms of "synapse" (GO:0045202, 99 out of 902 DEGs), "neuron projection" (GO:0043005, 103 out of 902 DEGs) and "somatodendritic compartment" (GO:0036477, 68 out of 902 DEGs) (Figure 5C, full list in Table S3). In total, 150 DEGs (56 upregulated and 94 downregulated, 17% of total DEGs) were defined as experience-induced Synaptic-CC DEGs (Figure 5D), among which more than 90% were dependent on the animals' behavioral experience in the spatial environment (128 genes not differentially regulated and 11 inversely regulated in the baseline condition). This was supported by a GO-BP analysis, showing a high overrepresentation of NEIL3-dependent DEGs in synaptic processes, such as regulation of trans-synaptic signaling (GO:0099177), synapse organization (GO:0050808) and their respective sub-terms (Figure 5E, full list in Table S4). A total of 62 DEGs were associated with synaptic processes, among which the majority (82%) were not recognized in *Neil3*$^{-/-}$ CA1 at baseline. Taken together, these results suggest a functional relevance of NEIL3 for the experience-induced synaptic regulation.

NEIL3 modulates spatial experience induced expression of immediate early genes

Immediate early genes (IEGs) have been identified as key components in synaptic plasticity and as cellular representations in neuronal ensembles underlying the memory trace/engram (Minatohara et al., 2015; Asok et al., 2019). Induced expression of IEGs such as *Arc* and *c-Fos* has been found in hippocampal CA1 neurons associated with neuronal activity during spatial learning (Guzowski et al., 1999, 2001, 2006; Vann et al., 2000). In our transcriptome data, we observed upregulation of several IEGs, including *Arc* and *c-Fos*, following spatial exploration (SE) in the wild type as well as *Neil3*$^{-/-}$ CA1, but no difference was observed between genotypes (Figure 6A). As Arc and c-Fos upregulation is usually observed in a small subset of hippocampal cells (Goode et al., 2020) while our RNAseq approach examined the entire population of CA1 neurons, we then tested whether quantitative genotype-dependent differences become visible in an IHC-approach visualizing single cells. Consistently, Arc^{+} and c-Fos^{+} cells were increased throughout the hippocampal CA1 in wild type mice after spatial exploration ($p < 0.0001$, two-way ANOVA). Strikingly, this immediate early gene response was significantly impaired in mice lacking NEIL3 ($p < 0.0001$, two-way ANOVA) (Figures 6B and 6C), suggesting a role of NEIL3 in modulating the expression of IEGs in response to spatial experience.

DISCUSSION

Here, we provide evidence that NEIL3 shapes the CA1 transcriptome during development and behavior, which is essential for the maturation and the functional plasticity of CA1 neurons. We characterized postnatal maturation of CA1 in *Neil3*$^{-/-}$ mice and identified functionally distinct DEGs across postnatal development. We analyzed functional properties of CA1 neurons and revealed impaired spatial stability in place cells lacking NEIL3. We explored spatial experience-induced gene expression and detected NEIL3-dependent gene modulation essential for synaptic regulation. Spatial-experience-induced expression of immediate early genes in *Neil3*$^{-/-}$ CA1 were confirmed by immunohistochemistry. Our work, for the first time, links NEIL3, a DNA repair enzyme, to the neural basis of spatial cognition, thus shedding light on the molecular determinants enabling a stable neural representation of space.

NEIL3 shapes CA1 transcriptome during postnatal maturation

The association of NEIL3 with transcriptional modulation has been recently reported. Dysregulated genes related to cardiovascular development and connective tissue disorders were identified in NEIL3-deficient hearts (Olsen et al., 2017). Our work revealed differentially regulated genes in *Neil3*$^{-/-}$ hippocampal CA1 region associated with hippocampal development. As a high degree of transcriptional variety has been delineated in subregions of the hippocampus (Datson et al., 2004; Thompson et al., 2008), we explored the role of NEIL3 in CA1-specific gene regulation during postnatal development. Whole transcriptomes were analyzed from carefully dissected dorsal CA1 samples of *Neil3*$^{-/-}$ mice at early postnatal age (p8), in which signs of delayed neuronal maturation was observed, and at adulthood (3 m), in which completed matured CA1 was expected. We applied a multifactorial analysis with interaction of age and genotype to characterize the differences in longitudinal patterns of gene expression in wild type and *Neil3*$^{-/-}$ CA1, that

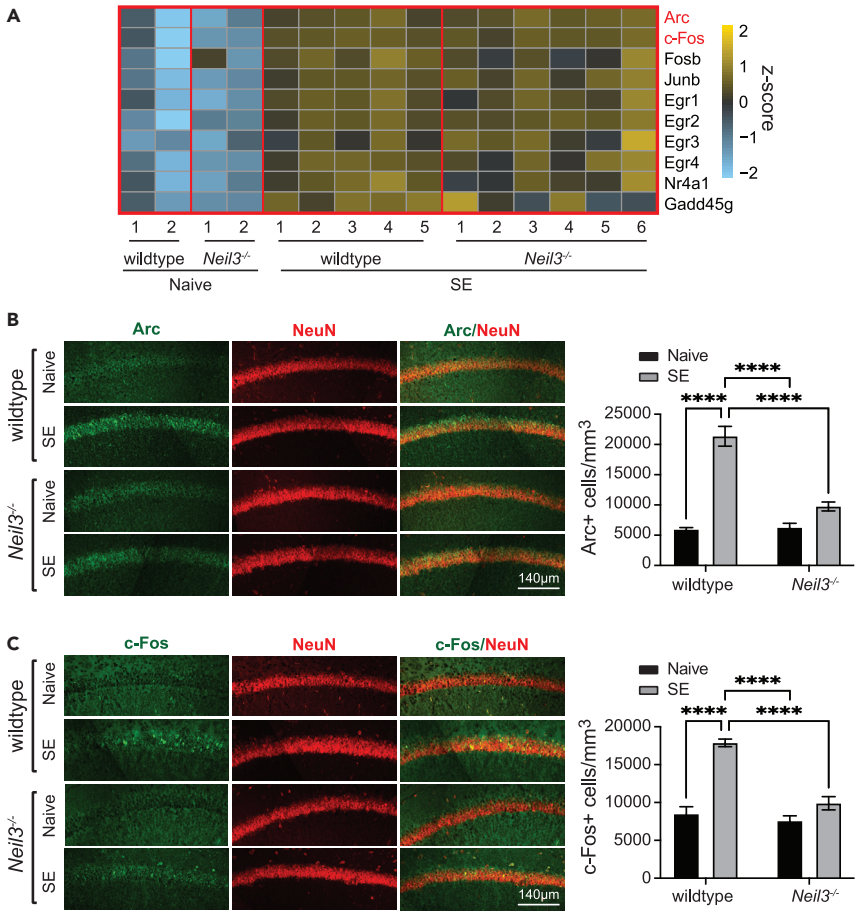

Figure 6. Spatial experience induced expression of immediate early genes in wildtype and *Neil3*$^{-/-}$ CA1 neurons

(A) Heatmap showing z-score normalized FPKM expression levels of selected immediate early genes (based on whole-CA1 RNAseq) from wt and *Neil3*$^{-/-}$ mice without (Naive) or after spatial exploration ("SE").

(B) Dorsal hippocampal CA1 was immunostained with antibodies against Arc (green) and NeuN (red). The number of Arc positive CA1 neurons in wildtype and *Neil3*$^{-/-}$ mice with or without behavior strained was analyzed.

(C) Similarly, dorsal hippocampal CA1 was immunostained with antibodies against c-Fos (green) and NeuN (red). The number of c-Fos positive CA1 neurons in wildtype and *Neil3*$^{-/-}$ mice with or without behavioral intervention was analyzed. Statistics were conducted at animal level (6 animals with 2 hippocampal slices for each genotype, two-way-ANOVA, Sidak's correction, error bars indicate mean ± SEM).

allows to pinpoint the NEIL3-dependent DEGs (Differentially Expressed Genes) not only at a particular postnatal timepoint but also that have a different direction of changes in expression across the postnatal timeline. NEIL3 per se expressed highly in the immature p8-CA1 but low at adulthood (Figure S3B), similar as observed in the previous study (Rolseth et al., 2008), implicating a role of NEIL3 in the CA1 development. The NEIL3-dependent, development-associated DEGs were highly enriched in neurobiological processes important for neurodevelopment, synaptic function, as well as learning and memory, suggesting an essential role of NEIL3 in shaping transcription in CA1 during its structural and functional maturation. Of note, the thematic classification as provided by Gene Ontology (GO) analysis refers to the projected function of the differentially expressed gene, not to the localization where the transcript was isolated.

Further, we defined a group of "Synaptic-CC DEGs" in *Neil3*$^{-/-}$ CA1 that were highly overrepresented in GO-CC terms essential for synaptic functions. The ones that had unique expression patterns in immature p8-CA1 were highly associated with biological processes such as "axon ensheathment", "neuron projection development" and "synapse organization and regulation" (Figure 2D), suggesting a role of NEIL3 in the structural maturation of neurons and neural networks. This is in line with previous studies that NEIL3 mainly functions in proliferating, immature cells (Sejersted et al., 2011; Regnell et al., 2012). The ones

that had unique expression patterns in mature CA1 (3 m) were highly associated with processes essential for synaptic transmission and signaling (Figure 2E), suggesting a role of NEIL3 in the synaptic regulation of mature, postmitotic neurons. Taken together, this result implicates that NEIL3 functions as a transcription modulator important for the structural and functional development of hippocampal circuits. NEIL3 has been implicated in epigenetic mechanisms involving DNA modifications as well as 3D-genome architecture that are critical for gene regulation (Zhou et al., 2013; Muller et al., 2014). The precise molecular interplay of NEIL3 with epigenetic marks during hippocampal development remains to be elucidated.

NEIL3 impacts functional plasticity of hippocampal place cells

Hippocampal place cells, as one of the most remarkable neuronal correlates for spatial cognition, have been widely studied to understand the memory mechanisms in the hippocampus. Place cells are selectively activated in a particular location of the environment (O'Keefe and Dostrovsky, 1971) and are able to keep the same firing pattern ("place field") for days and months, suggesting their encoding for long-term memory of a learned environment (Thompson and Best, 1990). Meanwhile, place cells often alter their firing patterns in response to environmental changes, suggesting their ability of dissociating the dissimilarities and generating new maps for a novel environment (Muller and Kubie, 1987; Bostock et al., 1991). In this study, we recorded the activity of neurons in the hippocampal CA1 region of wt and *Neil3*$^{-/-}$ mice while the animals were freely moving in an open field environment and examined whether NEIL3-deficient CA1 place cells are functionally normal.

Similar numbers of place cells were recorded in wild type and *Neil3*$^{-/-}$ CA1. No significant difference was observed in terms of firing rate, field size and the spatial information content. However, a higher fraction of place cells in *Neil3*$^{-/-}$ CA1 displayed multiple environment-specific firing fields (Figure 3F). *Neil3*$^{-/-}$ cells reliably remapped to the new environment as the wild type ones (Figures 4A, 4B, and S5B), indicating an intact ability to generate new maps. However, an increased fraction of *Neil3*$^{-/-}$ place cells kept remapping in the familiar environment when recorded at different trials with a 50 min or 24h interval (Figures 4B, 4D, and S5D), demonstrating an impaired long-term spatial stability. Of note, within each recording session, the place fields of *Neil3*$^{-/-}$ CA1 neurons were stable and coherent (table in Figure 3E), implying that *Neil3*$^{-/-}$ CA1 place cells reliably maintained the maps once they were selected. Interestingly, preserved within-session spatial stability and frequent remapping across trials were also observed in CA1 place cells of aged animals (Barnes et al., 1997; Schimanski et al., 2013), associating with the decreased spatial cognition during aging as observed in the behavior of *Neil3*$^{-/-}$ mice (Regnell et al., 2012). Future studies should therefore explore NEIL3-dependent mechanisms regulating the age-dependent decline of hippocampal functions.

NEIL3 impacts spatial experience-induced gene expression essential for synaptic regulation

Experience-dependent changes in transcription play a pivotal role in the plasticity of neurons and neural circuits for cognitive function and behavior (Yap and Greenberg, 2018). As NEIL3 was detected in adult CA1 (Figures S3A and S3B), we hypothesized that NEIL3 may directly impact the spatial experience-induced gene expression. Almost 2000 genes had statistically differential expression ($P_{adj} < 0.05$) in *Neil3*$^{-/-}$ CA1 after spatial exploration; however, more than 90% of genes had subtle transcriptional changes (ABS (log_2FC) < 0.6) (Figure 5B). This may be due to the behavioral setup we used: a spatial exploration paradigm in the open field leads to neuronal activation, which is less drastic than the learning induced plasticity response. To include all possible NEIL3-modulated genes that are potentially biologically relevant, we defined the experience-induced DEGs using a relatively low log_2FC threshold (ABS (log_2FC) $\geq$ 0.3). Again, these DEGs were highly overrepresented in GO-Cellular Component and GO-Biological Process essential for synaptic regulation suggesting a role of NEIL3 in modulating experience-induced synaptic plasticity. Of note, the differential regulation of distinct glutamate and GABA receptors was observed, for example, NMDA-type ionotropic glutamate receptor subunits, such as NR2A/*Grin2a* ($log_2FC = -0.45$) and NR2d/*Grin2d* ($log_2FC = -0.42$), metabotropic glutamate receptor mGluR2/*Grm2* ($log_2FC = -1.5$) as well as the alpha2 subunit of $GABA_A$ receptor GABRA2/*Gabra2* ($log_2FC = -1.62$) were all downregulated in *Neil3*$^{-/-}$ CA1 after spatial exploration. Downregulation of GABRA2 was verified by IHC and Western Blot in the adult CA1 of *Neil3*$^{-/-}$ mice with and without behavior intervention (Figure S7). Differential regulation of GABRA2/*Gabra2* and mGluR2/*Grm2* was also detected across development (Figure 2). Thus, NEIL3 may contribute to the regulation of neuronal excitability and synaptic transmission, which is critical for the hippocampal-dependent cognitive processes. Moreover, learning induces alterations not only at the level of synaptic physiology but also at chromatin organization (West

and Greenberg, 2011; Asok et al., 2019; Campbell and Wood, 2019). The impact of NEIL3 on experience-induced epigenomic changes should be further investigated.

NEIL3 modulates experience-induced immediate early genes in CA1 neurons

Immediate early genes (IEGs) such as *c-fos* and *Arc* are rapidly upregulated in subsets of neurons in response to sensory and behavioral experiences, allowing for the functional adaptation of these neurons and the storage of long-term memory (West and Greenberg, 2011; Minatohara et al., 2015; Asok et al., 2019). Recent studies describe progressively stabilized IEG activation patterns in distinct CA1 neuronal ensembles over repeated visits to the same environment for weeks, supporting that the long-term consolidation of hippocampal plasticity patterns is required for long-term memory formation (Attardo et al., 2018). We observed spatial exploration induced upregulation of several IEGs in wt and *Neil3*$^{-/-}$ CA1 (Figure 6A), which is consistent with the long-term stabilization of IEG activation patterns as previously described (Attardo et al., 2018). We did not detect quantitative differences of IEG transcripts between genotypes and no immediate transcriptional changes were observed in CA1 after novel-environment stimuli. As we extracted RNA from a pool of CA1 pyramidal neurons, this could be explained by sparse IEG activation in distinct subpopulation of neurons at CA1, although different environments evoked comparable levels of bulk IEG activity (Attardo et al., 2018; Goode et al., 2020).

By using immunochemistry and 3D image analysis, we found reduced induction of Arc and c-Fos in *Neil3*$^{-/-}$ CA1 neurons after spatial exploration (Figures 6B and 6C), suggesting that NEIL3 is involved in the maintenance of IEG-dependent ensemble neural plasticity for long-term memory. Arc^{+} and c-Fos^{+} neuronal ensembles in the hippocampus have been explored as engram cells that are associated with memory traces (Garner et al., 2012; Liu et al., 2012; Denny et al., 2014). An interesting future approach would thus be an activity-dependent memory tagging strategy allowing for the observation and reactivation of memory engrams (Goode et al., 2020), in order to delineate the interplay of NEIL3 and engram formation.

Limitations of the study

Our work provided evidence supporting an important role of NEIL3, a DNA repair enzyme, in neuronal maturation and function by shaping transcription. However, there were several limitations to the current study. First, we identified differentially expressed genes in NEIL3-depleted hippocampal neurons that were essential for synaptic development and function, but we did not establish a detailed molecular mechanism on how NEIL3 contributed directly to the synaptic regulation. Second, NEIL3 has been implicated in epigenetic mechanisms involving DNA modifications and 3D-genome architecture (Zhou et al., 2013; Muller et al., 2014), but we did not elucidate the molecular interplay of NEIL3 with epigenetic marks and transcription in hippocampal neurons. Third, our study was limited to a mouse model with a constitutive knockout of *Neil3*. It can be hypothesized that the impaired function of CA1 place cells was because of changes in the entire hippocampus or even whole brain networks after a complete NEIL3 depletion in mice.

STAR★METHODS

Detailed methods are provided in the online version of this paper and include the following:

- KEY RESOURCES TABLE
- RESOURCE AVAILABILITY
  - Lead contact
  - Materials availability
  - Data and code availability
- EXPERIMENTAL MODEL AND SUBJECT DETAILS
  - Subjects
- METHOD DETAILS
  - Spatial-exploration and behavioral paradigms
  - Dissection of CA1-specific brain tissue
  - RNAseq and analysis of differential gene expression
  - Surgical procedure
  - Neuronal recording procedures
  - Spike sorting and rate maps
  - Analysis of place cells
  - Histology and reconstruction of recording positions

- Immunohistochemistry
- Confocal imaging and 3D image analysis
- Real-time quantitative PCR
- Western blot

- QUANTIFICATION AND STATISTICAL ANALYSIS

SUPPLEMENTAL INFORMATION

Supplemental information can be found online at https://doi.org/10.1016/j.isci.2021.103470.

ACKNOWLEDGMENTS

We are grateful to Edvard Moser and May-Britt Moser for sharing the MATLAB code of place cell analysis and the access of NORBRAIN infrastructures in Trondheim, inspiring discussion, and critical reading of the manuscript. We appreciate feedback on the manuscript provided by Carol A. Barnes, Katja Scheffler and Barbara van Loon. We thank Menno Witter for inspiring discussion and technical support on neuroanatomy, Pål Sætrom for his critical thoughts in RNAseq analysis, Atle van Beelen Granlund and Bjørn Munkvold for sharing the laser dissection and cryostat equipment. This work was funded by the Research Council of Norway (RCN, FRIPRO 297037 and 287911) and the Central Norway Regional Health Authority (HMN 28363).

AUTHOR CONTRIBUTIONS

N.K. and J.Y. designed the experiments and contributed to data analysis. N.K. conducted all experiments. M.S.F.B. assisted on IHC studies and performed RT-qPCR and Western Blot experiments. A.M.B. analyzed the RNAseq data. P.B. contributed to extracellular recording of CA1 neurons. J.Y. and M.B. designed and supervised the research. N.K. drafted and J.Y. wrote the manuscript. M.B. and J.Y. acquired the funding.

DECLARATION OF INTERESTS

The authors declare no competing interests.

Received: June 2, 2021
Revised: September 16, 2021
Accepted: November 15, 2021
Published: December 17, 2021

REFERENCES

Asok, A., Leroy, F., Rayman, J.B., and Kandel, E.R. (2019). Molecular mechanisms of the memory trace. Trends Neurosci. *42*, 14–22.

Attardo, A., Lu, J., Kawashima, T., Okuno, H., Fitzgerald, J.E., Bito, H., and Schnitzer, M.J. (2018). Long-term consolidation of ensemble neural plasticity patterns in hippocampal area CA1. Cell. Rep. *25*, 640–650.e2.

Barnes, C.A., Suster, M.S., Shen, J., and McNaughton, B.L. (1997). Multistability of cognitive maps in the hippocampus of old rats. Nature *388*, 272–275.

Best, P.J., White, A.M., and Minai, A. (2001). Spatial processing in the brain: The activity of hippocampal place cells. Annu. Rev. Neurosci. *24*, 459–486.

Blighe, K., Rana, S., and Lewis, M. (2020). EnhancedVolcano: Publication-ready volcano plots with enhanced colouring and labeling. R package version 160. https://githubcom/kevinblighe/EnhancedVolcano.

Boccara, C.N., Sargolini, F., Thoresen, V.H., Solstad, T., Witter, M.P., Moser, E.I., and Moser, M.B. (2010). Grid cells in pre- and parasubiculum. Nat. Neurosci. *13*, 987–994.

Bostock, E., Muller, R.U., and Kubie, J.L. (1991). Experience-dependent modifications of hippocampal place cell firing. Hippocampus *1*, 193–205.

Campbell, R.R., and Wood, M.A. (2019). How the epigenome integrates information and reshapes the synapse. Nat. Rev. Neurosci. *20*, 133–147.

Cembrowski, M.S., and Spruston, N. (2019). Heterogeneity within classical cell types is the rule: Lessons from hippocampal pyramidal neurons. Nat. Rev. Neurosci. *20*, 193–204.

Datson, N.A., Meijer, L., Steenbergen, P.J., Morsink, M.C., van der Laan, S., Meijer, O.C., and de Kloet, E.R. (2004). Expression profiling in laser-microdissected hippocampal subregions in rat brain reveals large subregion-specific differences in expression. Eur. J. Neurosci. *20*, 2541–2554.

Denny, C.A., Kheirbek, M.A., Alba, E.L., Tanaka, K.F., Brachman, R.A., Laughman, K.B., Tomm, N.K., Turi, G.F., Losonczy, A., and Hen, R. (2014). Hippocampal memory traces are differentially modulated by experience, time, and adult neurogenesis. Neuron *83*, 189–201.

Eagle, A.L., Gajewski, P.A., and Robison, A.J. (2016). Role of hippocampal activity-induced transcription in memory consolidation. Rev. Neurosci. *27*, 559–573.

Garner, A.R., Rowland, D.C., Hwang, S.Y., Baumgaertel, K., Roth, B.L., Kentros, C., and Mayford, M. (2012). Generation of a synthetic memory trace. Science *335*, 1513–1516.

Goode, T.D., Tanaka, K.Z., Sahay, A., and McHugh, T.J. (2020). An integrated index: Engrams, place cells, and hippocampal memory. Neuron *107*, 805–820.

Guzowski, J.F., McNaughton, B.L., Barnes, C.A., and Worley, P.F. (1999). Environment-specific expression of the immediate-early gene Arc in hippocampal neuronal ensembles. Nat. Neurosci. *2*, 1120–1124.

Guzowski, J.F., Miyashita, T., Chawla, M.K., Sanderson, J., Maes, L.I., Houston, F.P., Lipa, P., McNaughton, B.L., Worley, P.F., and Barnes, C.A. (2006). Recent behavioral history modifies coupling between cell activity and Arc gene transcription in hippocampal CA1 neurons. Proc. Natl. Acad. Sci. U S A *103*, 1077–1082.

Guzowski, J.F., Setlow, B., Wagner, E.K., and McGaugh, J.L. (2001). Experience-dependent gene expression in the rat hippocampus after

spatial learning: a comparison of the immediate-early genes Arc, c-fos, and zif268. J. Neurosci. *21*, 5089–5098.

Henriksen, E.J., Colgin, L.L., Barnes, C.A., Witter, M.P., Moser, M.B., and Moser, E.I. (2010). Spatial representation along the proximodistal axis of CA1. Neuron *68*, 127–137.

Huber, W., Carey, V.J., Gentleman, R., Anders, S., Carlson, M., Carvalho, B.S., Bravo, H.C., Davis, S., Gatto, L., Girke, T., et al. (2015). Orchestrating high-throughput genomic analysis with Bioconductor. Nat. Methods *12*, 115–121.

Jung, M.W., and McNaughton, B.L. (1993). Spatial selectivity of unit activity in the hippocampal granular layer. Hippocampus *3*, 165–182.

Krokan, H.E., and Bjoras, M. (2013). Base excision repair. Cold Spring Harb Perspect. Biol. *5*, a012583.

Leutgeb, S., Leutgeb, J.K., Barnes, C.A., Moser, E.I., McNaughton, B.L., and Moser, M.B. (2005). Independent codes for spatial and episodic memory in hippocampal neuronal ensembles. Science *309*, 619–623.

Liu, X., Ramirez, S., Pang, P.T., Puryear, C.B., Govindarajan, A., Deisseroth, K., and Tonegawa, S. (2012). Optogenetic stimulation of a hippocampal engram activates fear memory recall. Nature *484*, 381–385.

Love, M.I., Huber, W., and Anders, S. (2014). Moderated estimation of fold change and dispersion for RNA-seq data with DESeq2. Genome Biol. *15*, 550.

Mi, H., Muruganujan, A., Huang, X., Ebert, D., Mills, C., Guo, X., and Thomas, P.D. (2019). Protocol update for large-scale genome and gene function analysis with the PANTHER classification system (v.14.0). Nat. Protoc. *14*, 703–721.

Minatohara, K., Akiyoshi, M., and Okuno, H. (2015). Role of immediate-early genes in synaptic plasticity and neuronal ensembles underlying the memory trace. Front. Mol. Neurosci. *8*, 78.

Muller, R.U., and Kubie, J.L. (1987). The effects of changes in the environment on the spatial firing of hippocampal complex-spike cells. J. Neurosci. *7*, 1951–1968.

Muller, R.U., and Kubie, J.L. (1989). The firing of hippocampal place cells predicts the future position of freely moving rats. J. Neurosci. *9*, 4101–4110.

Muller, U., Bauer, C., Siegl, M., Rottach, A., and Leonhardt, H. (2014). TET-mediated oxidation of methylcytosine causes TDG or NEIL glycosylase dependent gene reactivation. Nucleic Acids Res. *42*, 8592–8604.

O'Keefe, J. (1979). A review of the hippocampal place cells. Prog. Neurobiol. *13*, 419–439.

O'Keefe, J., and Dostrovsky, J. (1971). The hippocampus as a spatial map. Preliminary evidence from unit activity in the freely-moving rat. Brain Res. *34*, 171–175.

Olsen, M.B., Hildrestrand, G.A., Scheffler, K., Vinge, L.E., Alfsnes, K., Palibrk, V., Wang, J., Neurauter, C.G., Luna, L., Johansen, J., et al. (2017). NEIL3-dependent regulation of cardiac fibroblast proliferation prevents myocardial rupture. Cell Rep. *18*, 82–92.

Pan, L., Penney, J., and Tsai, L.H. (2014). Chromatin regulation of DNA damage repair and genome integrity in the central nervous system. J. Mol. Biol. *426*, 3376–3388.

Regnell, C.E., Hildrestrand, G.A., Sejersted, Y., Medin, T., Moldestad, O., Rolseth, V., Krokeide, S.Z., Suganthan, R., Luna, L., Bjoras, M., et al. (2012). Hippocampal adult neurogenesis is maintained by Neil3-dependent repair of oxidative DNA lesions in neural progenitor cells. Cell Rep *2*, 503–510.

Rolseth, V., Luna, L., Olsen, A.K., Suganthan, R., Scheffler, K., Neurauter, C.G., Esbensen, Y., Kusnierczyk, A., Hildrestrand, G.A., Graupner, A., et al. (2017). No cancer predisposition or increased spontaneous mutation frequencies in NEIL DNA glycosylases-deficient mice. Sci. Rep. *7*, 4384.

Rolseth, V., Runden-Pran, E., Luna, L., McMurray, C., Bjoras, M., and Ottersen, O.P. (2008). Widespread distribution of DNA glycosylases removing oxidative DNA lesions in human and rodent brains. DNA Repair (Amst) *7*, 1578–1588.

Scheffler, K., Bjoras, K.O., and Bjoras, M. (2019). Diverse functions of DNA glycosylases processing oxidative base lesions in brain. DNA Repair (Amst) *81*, 102665.

Schimanski, L.A., Lipa, P., and Barnes, C.A. (2013). Tracking the course of hippocampal representations during learning: when is the map required? J. Neurosci. *33*, 3094–3106.

Sejersted, Y., Hildrestrand, G.A., Kunke, D., Rolseth, V., Krokeide, S.Z., Neurauter, C.G., Suganthan, R., Atneosen-Asegg, M., Fleming, A.M., Saugstad, O.D., et al. (2011). Endonuclease VIII-like 3 (Neil3) DNA glycosylase promotes neurogenesis induced by hypoxia-ischemia. Proc. Natl. Acad. Sci. USA *108*, 18802–18807.

Spruijt, C.G., Gnerlich, F., Smits, A.H., Pfaffeneder, T., Jansen, P.W., Bauer, C., Munzel, M., Wagner, M., Muller, M., Khan, F., et al. (2013). Dynamic readers for 5-(hydroxy)methylcytosine and its oxidized derivatives. Cell *152*, 1146–1159.

Thompson, C.L., Pathak, S.D., Jeromin, A., Ng, L.L., MacPherson, C.R., Mortrud, M.T., Cusick, A., Riley, Z.L., Sunkin, S.M., Bernard, A., et al. (2008). Genomic anatomy of the hippocampus. Neuron *60*, 1010–1021.

Thompson, L.T., and Best, P.J. (1990). Long-term stability of the place-field activity of single units recorded from the dorsal hippocampus of freely behaving rats. Brain Res. *509*, 299–308.

Vann, S.D., Brown, M.W., Erichsen, J.T., and Aggleton, J.P. (2000). Fos imaging reveals differential patterns of hippocampal and parahippocampal subfield activation in rats in response to different spatial memory tests. J. Neurosci. *20*, 2711–2718.

von Bohlen Und Halbach, O. (2007). Immunohistological markers for staging neurogenesis in adult hippocampus. Cell Tissue Res. *329*, 409–420.

West, A.E., and Greenberg, M.E. (2011). Neuronal activity-regulated gene transcription in synapse development and cognitive function. Cold Spring Harb. Perspect. Biol. *3*, a005744.

Wu, X., and Zhang, Y. (2017). TET-mediated active DNA demethylation: Mechanism, function and beyond. Nat. Rev. Genet. *18*, 517–534.

Yap, E.L., and Greenberg, M.E. (2018). Activity-regulated transcription: Bridging the gap between neural activity and behavior. Neuron *100*, 330–348.

Zhou, J., Liu, M., Fleming, A.M., Burrows, C.J., and Wallace, S.S. (2013). Neil3 and NEIL1 DNA glycosylases remove oxidative damages from quadruplex DNA and exhibit preferences for lesions in the telomeric sequence context. J. Biol. Chem. *288*, 27263–27272.

STAR★METHODS

KEY RESOURCES TABLE

REAGENT or RESOURCE	SOURCE	IDENTIFIER
Antibodies		
Anti-c-fos, rabbit polyclonal	Synaptic Systems	Cat. No. 226003 RRID: AB_2231974
Anti-Arc, rabbit polyclonal	Synaptic Systems	Cat. No. 156002 RRID: AB_887695
Anti-NeuN, mouse monoclonal (A60, MAB377)	Merck Millipore	Cat. No. 636574 RRID: AB_2298772
Anti-GABRA2, rabbit polyclonal	Synaptic Systems	Cat. No. 224103 RRID: AB_2108839
Anti-Tubb3/Tuj1, mouse IgG2a	R&D Systems	Cat. No. MAB1195, RRID: AB_357520
Alexa Fluor 488 anti-rabbit	ThermoFisher	Cat. No. A32731 RRID: AB_2633280
Alexa Fluor 488 anti-mouse IgG2a	ThermoFisher	Cat. No. A-21131 RRID: AB_2535771
Alexa Fluor 555 anti-mouse IgG1	ThermoFisher	Cat. No. A-31570 RRID: AB_2536180
Anti-GABRA2,	Thermofisher	Cat. No. MA5-27702 RRID: AB_2735191
GAPDH-HRP, mouse monoclonal (GA1R)	Thermofisher	Cat. MA5-15738-HRP RRID: AB_2537659
Goat-anti-mouse-HRP	Agilent/DAKO	Cat. No. P0447 RRID: AB_2617137
Chemicals, peptides, and recombinant proteins		
Platinum black plating solution	Neuralynx	Neuralynx.com
Meliodent Væske kald 500 mL	K. A. Rasmussen	Cat. No. 800120
Meliodent Kald Transpa 01 1 kg	K. A. Rasmussen	Cat. No. 800108
Histoacryl sealant 0.5 g	BRAUN	Cat. No. 1050052B
Isoflurane anesthetic agent	Baxter	Cat.No. 1001936060
Cresyl violet Acetate	Sigma-Aldrich	Cat. No. C5042
DAPI solution (1 mg/mL)	ThermoFisher	Cat. No. 62248
ProLong™ Gold Antifade Mountant with DAPI	ThermoFisher	Cat. No. P36935
ProClin preservative agent	Sigma-Aldrich	Cat. No. 49379-U
Power SYBR© green PCR master mix	Applied Biosystems	Cat. No. 4367659
RIPA lysis and Extraction buffer	ThermoFisher	Cat. No. 89900
Protease & phosphatase inhibitor Cocktail 100X	ThermoFisher	Cat. No. 1861280
Bio-rad protein assay dye reagent	BIO-RAD	Cat. No. 5000006
NuPAGE LDS sample buffer	Invitrogen	Cat. No. NP0007
NuPAGE 4-12% Bis-Tris gel	Invitrogen	Cat. No. NP0323BOX
NuPAGE MOPS SDS running buffer	Invitrogen	Cat. No. NP0001-02
SeeBlue Plus2 Prestained standard ladder	Invitrogen	Cat. No. LC5925
Ponceau S	Sigma-Aldrich	Cat. No. P3504-100G
SuperSignal west femto maximum stable peroxide buffer	ThermoFisher	Cat. No. 1856190
SuperSignal west femto maximum luminol enhancer solution	ThermoFisher	Cat. No. 1856189

(*Continued on next page*)

Continued

REAGENT or RESOURCE	SOURCE	IDENTIFIER
Critical commercial assays		
AllPrep DNA/RNA/Protein extraction kit	Qiagen	Cat. No. 80204
RNeasy mini RNA extraction kit	Qiagen	Cat. No. 74104
High-capacity cDNA reverse transcription kit	Qiagen	Cat. No. 4368813
Deposited data		
GEO database	https://www.ncbi.nlm.nih.gov/geo/	GSE175358 GSE148408
Mendeley data	https://data.mendeley.com/datasets/whybmf976p/1	https://doi.org/10.17632/whybmf976p.1
Experimental models: Organisms/strains		
Neil3$^{-/-}$ mutant mice	Own breed, Genoway, Sejersted et al., 2011	Gene ID 234258
C57Bl6N wildtype mice	Own line/Janvier Labs	Bx 239294
Software and algorithms		
DESeq2	Love et al. (2014)	https://bioconductor.org/packages/release/bioc/html/DESeq2.html RRID:SCR_015687
R "dark and stormy night"	Open source	r-project.org RRID:SCR_001905
Panther database	Open source	pantherdb.org RRID:SCR_004869
Gene ontology database	Open source	geneontology.org RRID:SCR_006941
Imaris 9.3	Bitplane	Bitplane.com RRID:SCR_007370
Tint graphical clustering software	Axona	axona.com
dacqUSB	Axona	axona.com
GraphPad prism 8.x (several versions used)	GraphPad Software	graphpad.com RRID:SCR_002798
ImageJ (version 2.1.0)	Fiji	RRID:SCR_002285
Other		
Cryostat/microtome	Leica, Germany	Leica CM3050S
Agilent BioAnalyzer	Agilent	BioAnalyzer 2100
Laser dissection microscope	MMI/Olympus	Olympus IX71/MMI
Zeiss LSM880 confocal microscope	Carl Zeiss	zeiss.com
StepOnePlus real-time PCR system	Applied Biosystems	Cat. No. 4376600
ChemiDoc MP imaging system	BIO-RAD	Cat. No. 12003154

RESOURCE AVAILABILITY

Lead contact

Further information and requests for resources and reagents should be directed to and will be fulfilled by the Lead Contact, Jing Ye (jing.ye@ntnu.no).

Materials availability

This study did not generate new unique reagents.

Data and code availability

All RNA sequencing data of this study have been deposited for public access in the NIH database Gene Expression Omnibus (GEO). Accession codes are GEO Dataset: GSE175358 (for the transcriptome data across development) and GEO Dataset: GSE148408 (for the transcriptome data after behavior). Recording datasets of wildtype and *Neil3*$^{-/-}$ hippocampal CA1 neurons have been deposited for public access in Mendeley Data: https://doi.org/10.17632/whybmf976p.1. Both GEO accession numbers and Mendeley DOI number are listed in the key resources table.

This paper does not report original code. All data reported in this paper will be shared by the lead contact upon reasonable request.

Any additional information required to reanalyze the data reported in this paper is available from the lead contact upon request.

EXPERIMENTAL MODEL AND SUBJECT DETAILS

Subjects

3-6 months old wildtype (C57Bl6N) and *Neil3*$^{-/-}$ mice (males) with an approximate body weight of 35 ± 3g were used for all experiments. *Neil3*$^{-/-}$ mice were generated and described previously (Sejersted et al., 2011). Animals were housed with their littermates in 1717 × 545 × 2045 mm (LxWxH) cages with free food and water access in a dedicated housing room (temperature 22°C ± 1°C and humidity 55% ± 5%) with a 12h light/dark cycle (lights on 7 pm to 7 am). Implanted animals were housed individually after surgery with food and water ad libitum and monitored daily during the experimental period. Behavior and neuronal recording experiments were performed in the dark phase. All experiments were conducted in accordance with the Norwegian Animal Welfare Act and approved by the Norwegian Animal Research Authority (FOTS11659).

METHOD DETAILS

Spatial-exploration and behavioral paradigms

As for assessing the experience-dependent transcriptome, wildtype and *Neil3*$^{-/-}$ mice were habituated in the open field of familiar environment (Room A, 50 × 50 cm plastic box with 30cm height of black walls and an A6-sized white cue card fixed at the north side constantly, dim light) with cues and food rewards for 20 min daily in a sequence of 7 days. The box rested on a table at a height of 100cm and surrounded by black curtains and the animal entered the environment from a constant side. After every exposition to the spatial exploration paradigm, the open field area was cleaned. On the test day (Day 7), half of the animals from each genotype were exposed in the familiar environment for 20 min, then rested for another 20 min before termination. The other half of the animals from each genotype were tested in a novel open field environment (Room B, 50 × 50 cm plastic box with 30cm height of white walls and an A6-sized black cue card fixed at the north side constantly, dim light) for 20 min, then rested for another 20 min before termination. As for the IHC studies, wildtype and *Neil3*$^{-/-}$ mice were only exposed to the familiar open field environment (20 min/training, 7 days) and terminated 40 min after the last test in Day7. As for the extracellular neuronal recording experiments, animals were habituated and recorded in the familiar open field environment in Room A and tested in a novel open field in Room B.

Dissection of CA1-specific brain tissue

The brain was taken out from the mouse without intracardial perfusion, mounted on a cryostat metal socket (Leica CM3050S) using a drop of mounting media (Tissue-Tek OCT compound), immediately frozen using pulverized dry ice (101 Cold Spray) and kept on dry ice until further processing. We established a needle-scratch method to precisely isolate hippocampal subregions with little prone to contamination from adjacent anatomical area (Figure S2). Coronal brain sections were frozen sectioned at a thickness of 100μm and mounted immediately onto gelatine-coated slides (SuperFrost Plus, ThermoFisher). After drying for 10-15min, subregions of the hippocampus (CA1, CA3 or DG) were scratched with a 30G needle (B.Braun) and collected in a dissection cap (MMI). CA1 samples were lysed in RLT lysis buffer (AllPrep Kit, Qiagen) using a bead homogenizer (MagNA lyser, Roche) and frozen at −80°C until further processing. As for the laser dissection method, a thickness of 8μm coronal brain sections were collected and mounted immediately on membrane slides (Molecular Machines and Industries GmbH). Typically, we mounted 5-6 slices per slide and collected a total of 20 slides for tissue isolation per animal, which usually comprised the entire

rostro-caudal axis of the hippocampal formation. Brain slices were stained using a modified cresyl violet fast-staining procedure, including sequential steps (*i*) dehydration (7 dips each in 70%, 80%, 90%, 100% EtOH), (*ii*) tissue clearance in Xylene for 1min, (*iii*) rehydration in cresyl violet solution for 90s without motion, (*iv*) final dehydration and clearance in xylene, (*v*) drying for 15-20min. The hippocampal CA1 pyramidal layer was dissected using a laser dissection microscope (Molecular Machines and Industries, CellCut on Olympus IX71) and collected in a dissection cap (MMI, Eching, Germany). We collected 20 CA1 dissectates in one isolation cap and finished one animal within the day.

RNAseq and analysis of differential gene expression

RNA was extracted using either the AllPrep Kit or the RNeasy Mini Kit from Qiagen according to the manufacturer's instructions. RNA samples typically yielded >100ng of RNA with a RIN value of >7 as determined by Bioanalyzer (Agilent Technologies). Whole-transcriptome sequencing was done by BGI Genomics Co., Ltd., Hong Kong, China. The samples were sequenced with BGISEQ-500 platform with the read depth 20M clean reads per sample, averagely generating about 4.92 Gb bases per sample. The sequencing reads containing low-quality, adaptor-polluted and high content of unknown base (N) reads were processed and removed. The clean data were provided by BGI and the bioinformatic analysis was performed in our lab.

Based on the sequencing results from BGI, the differential gene expression analysis was performed in R version 4.0.3 (2020-10-10), Platform: i386-w64-mingw32/i386 (R Core Team, 2019), Bioconductor ver. 3.10 (Huber et al., 2015) using DESeq2 ver. 1.26.0 (Love et al., 2014). In short, the package DESeq2 provides methods to test for differential expression by use of negative binomial generalized linear models; the estimates of dispersion and logarithmic fold changes incorporate data-driven prior distributions. For the multifactorial analysis of developmental sample set, the model with interaction was used (~genotype + age + genotype:age) and 5 result tables were generated: (*i*) DEGs in wildtype CA1 across ages (3m vs p8), (*ii*) DEGs in *Neil3*$^{-/-}$ CA1 across ages (3m vs p8), (*iii*) DEGs in immature CA1 (p8) across genotypes (*Neil3*$^{-/-}$ vs wildtype), (*iv*) DEGs in mature CA1(3m) across genotypes (*Neil3*$^{-/-}$ vs wildtype), and (*v*) DEGs with significant interaction of both age and genotype (the different expression patterns in *Neil3*$^{-/-}$ CA1 in the trajectory of development). To visualize the results volcano plot was generated using EnhancedVolcano (Blighe et al., 2020) and heatmaps of FPMK values were generated using the R package pheatmap: Pretty Heatmaps, version 1.0.12.

To determine differentially expressed genes (DEGs), the threshold of adjusted p value was set to 0.05 and the threshold of ABS ($\log_2$ Fold Change) was set to 0.6 (age-dependent transcriptome in Figure 1) or 0.3 (experience-dependent transcriptome in Figure 5). The number of animals used for this study was (*i*) p8 and adult CA1 transcriptome (Figures 1 and 2), n = 4 per genotype at p8, n = 3 per genotype at 3m, (*ii*) transcriptome "spatial exploration" condition (Figure 5), n = 5 for wildtype, n = 6 for *Neil3*$^{-/-}$, (*iii*) "baseline" condition in supplement (Figure S7), n = 2 per genotype. For the Gene Ontology (GO) over-representation analysis, the list of DEGs was uploaded to the online version of PANTHER Classification System (15.0, released 2020-07-28) using Binomial test and Bonferroni correction as well as mouse genome as background (Mi et al., 2019). The test was performed for each functional category (GO Ontology database released 2020-09-10): Cellular Compartment and Biological Process.

Surgical procedure

Mice were anesthetized using constant isoflurane application throughout the surgical procedure (0.5-1% isoflurane with an air flow at 2000 mL/min). A weight-adapted dose of buprenorphine (Temgesic, Indivior) was given either intraperitoneally or subcutaneously at least 15min prior to the first incision. A local dose of bupivacaine (Marcain, Aspen) was injected subcutaneously in the incision area of the mouse scalp. A prophylactic, weight-adapted dose of meloxicam (Metacam, Boehringer-Ingelheim Vetmedica) was given 15min before the end of the surgical procedure. Throughout surgery, eyes were protected using moisturizing eye cream (ViscoTears, Thea Pharma). Post-operative pain was controlled using buprenorphine and/or meloxicam according to the animal's need as assessed by a combined score of facial grimaces, behavior, fur state and weight.

A microdrive with an assembly of four tetrodes (sixteen electrodes) was inserted into the right hemisphere above the CA1 area of the dorsal hippocampus (stereotactic coordinates: AP[Bregma]: 2mm, ML: 1.8mm, DV: 0.8mm). The electrodes were made of 17-mm polyimidecoated platinum-iridium (90 to 10%) wire (California Fine Wire Co.) and plated with platinum (Platinum Black Plating Solution, Neuralynx, Inc.) to reduce

electrode impedances to ~200 kWat 1 kHz. A high-speed drill (Model1474, David Kopf Instruments) was used to penetrate the skull right above the area of tetrode insertion. Using a 27G needle (Sterican, B.Braun), the dura was gently nicked but not removed to allow the tetrode entering the neurocranium with ease. A metal 19G metal cannula was placed around the tetrode, resting loosely on the dura. The area of bone removal was kept moist using dental sponge (Spongostan Dental, Ethicon) soaked in saline 0.9% (B.Braun). A jeweler's screw was fixed to the skull serving as a ground electrode. The Microdrive and ground screw were fixed to the skull using dental cement.

Neuronal recording procedures

Mice were exposed to an open field environment (50 × 50 cm plastic box with 30cm height of black walls) 3 days after implantation and neuronal activities were recorded one week later when tetrode turning was started. The implanted microdrive was connected to the recording equipment (Axona Ltd.) via AC-coupled unity-gain operational amplifiers, using a counterbalanced cable that allowed the animal to move freely in the recording box. Recording data from HPC were collected using DacqUSB software from Axona. Recorded signals were amplified 8000 to 25,000 times and band-pass filtered between 0.8 and 6.7 kHz. The recording system tracked the position of two light-emitting diodes (infrared LEDs, one large and one small, 5 cm length) on the head stage (weight 5.12g) using an overhead video camera. Neuronal activity was recorded while the animal was freely moving in the recording box for a duration of 20 min. The behavior of mice was motivated by crumbs of chocolate loops randomly scattering in the open field area. The tetrodes were lowered in steps of 25 μm until single neurons could be isolated at appropriate depths. When putative place cells were observed, the remapping of place cells was monitored following five sequential sessions in the familiar and novel open field environment (Figure 4A). In between the recording sessions, mice were rest in a clean cage (30 × 20 cm transparent plastic box) for about 3 min. After collection of each data set, the tetrodes were moved further until new well-separated place cells were encountered. CA1 place cells were recorded in a DV-depth of 0.8-1.4 mm in mice.

Spike sorting and rate maps

The offline graphical cluster-cutting software Tint (Axona Ltd.) was used for spike sorting. The software provided a multidimensional parameter space consisting of two-dimensional projections with spike wave amplitudes and waveform energies, which were used to sort spikes and identify spike clusters belonging to one cell. Autocorrelation and cross-correlation functions were used as additional criteria to separate individual cell clusters reliably. Animal's position data were estimated based on the tracking of the two LEDs connecting to the head stage and the microdrive. All data were speed filtered, including spikes only when the animal had an instantaneous running speed of 2-100 cm/s. As described previously (Boccara et al., 2010), the distribution of firing rates was determined by the number of spikes as well as the time spent in each bin (2.5 × 2.5 cm) of the recording area (50 × 50cm). A 21-sample boxcar window filter (400ms, 10 samples on each side) was used for smoothing the recorded path. Additional smoothing using a quasi-Gaussian kernel over the surrounding 5 × 5 bins was applied to generate maps of spike number and time. The quotient of spike number and time for each bin of the smoothed map was used for defining the firing rate, with the bin showing the highest rate defined as the ''peak rate''.

Analysis of place cells

Place cells were defined by comparing each cell's spatial information score with the distribution of information scores for rate maps generated from randomly shuffled data as previously described (Henriksen et al., 2010). The chance level for spatial information was determined by a random shuffling procedure. The shuffled data are generated by time-shifting the entire sequence of spikes fired by one cell along the path of the animal: Each time shift equaled a random interval of a minimum of 20s and a maximum of the entire trial length minus 20s (in our case 1200s–20s = 1180s), with the end of each trial wrapped to the beginning. The shuffling procedure was repeated 100 times for each of the 419 cells recorded in the wildtype mice, yielding a total of 41,900 permutations and each of 402 cells recorded in the *Neil3*$^{-/-}$ mice, yielding a total of 40,200 permutations. A rate map was generated for each permutation and the distribution of spatial information values across all permutations of all cells was determined. The 95th percentile (see Figure 3) was used as a threshold to define place cells.

A place field was defined as an area equaling/larger than 50 cm^2 (8 or more 2.5 cm × 2.5 cm bins) where the firing rate was above 20% of the peak rate. Only place fields with a peak firing rate of at least 1Hz as well as a minimum of 100 spikes were included in the analysis. Interneurons and bypassing axons were defined by an

average peak-to-trough waveform duration of less than 200μs and excluded from the analysis. Spatial coherence was estimated as the first-order spatial autocorrelation of the smoothed rate maps, i.e. the mean correlation between firing rate of each bin and the averaged firing rate in the eight adjacent bins (Muller and Kubie, 1989). In-session spatial stability was calculated by the spatial correlation of place field maps from the first and second half of the open field trial. The spatial correlation between trials was determined for individual cells as previously described (Leutgeb et al., 2005; Henriksen et al., 2010). In brief, the rates of firing in corresponding bins of smoothed rate maps were correlated with one another, leading to a correlation procedure containing both the localization and number of spikes as the core variables. Correlation coefficients were calculated based on the full trial. Only place cells passing the 95th percentile criteria were included in the analysis. A population-based (1 cell = 1 statistical unit) analysis was applied, but only reported results as significant that passed a $p < 0.05$ in a nested t-test (1 animal = 1 statistical unit). The statistical analysis was conducted using GraphPad Prism Version 8.

Histology and reconstruction of recording positions

Electrodes were not moved after the final recording session. Mice were terminated using a combination of isoflurane (Baxter) and pentobarbital (>200mg/kg bodyweight) and then transcardially perfused with saline 0.9% followed by 4% paraformaldehyde. The electrodes were turned all the way up before the brain was extracted. Brains were quickly frozen and sectioned by a cryostat (Leica CM3050S, tempered to −25°C) at a thickness of 30μm in the sagittal plane. All sections around the area of the tetrode trace were collected and mounted on histological glass slides (SuperFrost). Slides were left to dry at room temperature overnight, stained using a standard cresyl violet staining protocol and imaged.

Immunohistochemistry

Sagittal brain sections (30 μm) were collected by frozen sectioning. Sections were incubated in antigen retrieval buffer (40mM trisodium citrate, pH6.0) at 99°C for 3 min. After washing in PBS, sections were pre-incubated in the blocking buffer (PBS with 5% normal goat serum, 1% BSA, and 0.1% Triton X-100) at room temperature for 2 h and then incubated with the diluted primary antibodies in dilution buffer (PBS with 1% normal goat serum, 1% BSA, and 0.1% Triton X-100) at 4° overnight. The next day, sections were washed 3 times in 1xPBST and incubated with the diluted secondary antibodies at room temperature for 2 h. After 3 times washing in 1x PBST, sections were mounted onto glass slides and dry overnight. Lastly, sections were incubated with DAPI (1μg/mL in PBS), washed and cover-slipped with mounting oil (ProLong™ Gold Antifade Mountant with DAPI, ThermoFisher). First antibodies are the ones against NeuN (mouse IgG1 1:500, Merck Millipore, Cat. No. MAB377), c-fos (rabbit IgGs 1:1000, Synaptic Systems, Cat. No. 226002), Arc (rabbit IgGs 1:1000, Synaptic Systems, Cat. No. 156002), Tubb3/Tuj1 (mouse IgG2a 1:500, R&D Systems, Cat. No. MAB1195) and GABRA2 (rabbit IgGs 1:1000, Synaptic systems, Cat. No. 224103). Secondary antibodies are from ThermoFisher: Alexa Fluor 488 anti-rabbit (1:1000, Cat. No. A32731), Alexa Fluor 555 anti-mouse IgG1 (1:1000, Cat. No. A-31570) and Alexa Fluor 488 anti-mouse IgG2a (1:1000, Cat. No. A-21131).

Confocal imaging and 3D image analysis

All fluorescent images were taken by confocal microscope (Zeiss LSM880). For synaptic markers (e.g. GABRA2), a Plan-Apochromat 40x/1.4 Oil DIC M27 objective was used. The size of the image window was 700 × 700μm (x/y 2000pixels of 0.35μm) and a z-interval of 0.5μm was applied. The distal and proximal part of the CA1 was imaged based on NeuN and DAPI staining as an anatomical orientation. For immediate early gene immunohistochemistry, a Plan-Apochromat 20x/0.8 M27 objective was used, a z-plane interval of 2μm was deemed sufficient to identify whole cells. The entire CA1 region was imaged as a region of interest based on NeuN and DAPI staining as an anatomical orientation.

We used the analysis software Imaris 9.3 (Bitplane, Zurich, Switzerland) to analyze fluorescent signals in 3D images. The strata pyramidale were identified as regions of interest using the "surface" tool. Based on the surface selection, a 3D-frame was created and the parameter of interest "masked" according to this frame. NeuN-positive cells at CA1 (Figures 1A, S1B, and S1D) as well as c-Fos and Arc positive cells (Figure 6) were identified within the masked channel using the tool of "Spots Wizard" in Imaris. A spot size of 5μm diameter was selected to spot individual cells. The "spot detection" tool relies on a local contrast/background subtraction-based approach, thus including only cells whose IHC-signal is clearly different from the surrounding background. As for the analysis of NeuN-positive mature neurons, Imaris plots the number of cells versus the mean intensity of the fluorescent signal in a histogram-like plot as schematically illustrated in Figure S1B. As stated in the figure, we used the point of the steepest rise in intensity between fractions as a

demarcation for the threshold between low- and high-intensity of NeuN staining (i.e. where the ascent "m" in y = m · x + t is largest). In other words, this point in the histogram represents a sharp 'jump' in mean intensity (dashed line in the schematic illustration) between cell populations, corresponding to a standardized, unarbitrary definition of what our eyes would identify as the likely border between low- and high-intensity NeuN reactivity. Effectively, the absolute threshold between populations can vary between single images, allowing for a flexible yet consistent way of defining the border between cell populations even if mean intensity values have minor variations due to unavoidable, small variations in immunohistochemistry staining efficiency and confocal microscopy signal detection. The similar approach was used to quantify Tubb3-positive immature neurons (Figure S1E). As for the analysis of GABRA2 (Figure S8), the "Spots Wizard" in Imaris was used to model areas of synaptic reactivity within this masked channel (1μm spot diameter for bouts of synaptic reactivity). After visual inspection of the modelled signal for biological relevance, the threshold for Quality Filter (see bitplane.com/imaris) was defined and kept throughout the analysis. Background subtraction was done for every specimen analyzed to account for intensity variations despite identical immunohistochemistry and confocal parameters. Whenever only one variable differed between groups, Student's t-test with Welch's correction was used. Considering the factors *genotype (wildtype vs. *Neil3*$^{-/-}$) and *intervention ("Naïve" vs. "SE") two-way-ANOVA was used with Sidak's correction for multiple testing. All comparisons were conducted with 1 animal equaling 1 statistical unit (2-3 sections per animal and 6 animals per genotype, both at "Naive" and "SE") and the analysis was conducted using GraphPad Prism Version 8.

Real-time quantitative PCR

cDNA was synthesized from 300ng of RNA, extracted from micro-dissected CA1, using the High-Capacity cDNA Reverse Transcription kit (Applied Biosystems, Thermo Fisher Scientific). Quantitative real-time PCR was performed in 10-μL reactions containing 3 ng of cDNA using the Power SYBR Green PCR master mix and the Step One Plus real-time PCR system (both from Applied Biosystems) according to the system and kit instructions. Relative gene expression was calculated using the comparative CT method. The expression of glyceraldehyde-3-phosphate dehydrogenase (Gapdh) mRNA were used as an internal control. The data presented are relative Neil3 mRNA levels. Primers used: mouse Gapdh, forward 5′-TCG TCC CGT AGA CAA AAT GGT-3′'-, reverse 5′-CGC CCA ATA CGG CCA AA-3′. Mouse Neil3, forward 5′-GGG CAA CAT CAT CAA AAA TGA A-3′, reverse 5′-CTG TTT GTC TGA TAG TTG ACA CAC CTT-3′.

Western blot

Micro-dissected hippocampal CA1 tissue samples were homogenized in RIPA buffer (ThermoFisher, Cat. No. 89900) with protease and phosphatase inhibitors (ThermoFisher, Cat. No. 1861280), using 1.4mm Zirconium oxide Beads (Precellys, Cat. No. P000927-LYSK0-A.0) with a spin of 5000rpm for 10 s in a MAGNAlyser Rotor (Roche Cat. No. 03359093001). Followed by centrifugation at 13,000 rpm for 20 min (4°C), the supernatant was collected, and the protein concentration was measured by the Bradford method using Bio-Rad Protein Assay Dye Reagent (Cat. No. 5000006). Proteins from 7.5 ug of total lysates were separated on 4–12% Bis-Tris NuPAGE gel (Invitrogen, Cat. No. NP0323BOX) by electrophoresis and transferred to nitrocellulose membrane using the Trans-Blot Turbo system (BIO-RAD, Cat. No. 1704158). After a 2-h blocking in skimmed milk at room temperature, the membrane was incubated with antibodies against GABRA2 (1:5000 in 5% of BSA, Thermofisher, Cat. No. MA5-27702) overnight at 4°C, then with Goat-Anti-Mouse-HRP Immunoglobulins (1:10,000 in PBST, Agilent/DAKO Cat. No. P0447) at room temperature for 1 h and imaged using ChemiDoc MP Imaging System (BIO-RAD, Cat. No. 12003154). The GAPDH-HRP antibody (1:10,000 in PBST, ThermoFisher, Cat. No. MA5-15738-HRP) was used as an internal control. The image was analyzed using the Analyze Gel tool in FIJI (ImageJ, version 2.1.0).

QUANTIFICATION AND STATISTICAL ANALYSIS

As for the transcriptome study, the differential gene expression analysis was performed using DESeq2 (ver. 1.26.0), which incorporates statistical methods and models that allow and facilitate analysis of small sample numbers (Love et al., 2014). The number of animals used in this study was: (*i*) p8 and adult CA1 transcriptome (Figures 1 and 2), n = 4 per genotype at p8, n = 3 per genotype at 3m, (*ii*) transcriptome "spatial exploration" condition (Figure 5), n = 5 for wildtype, n = 6 for *Neil3*$^{-/-}$, (*iii*) "baseline" condition in supplement (Figure S7), n = 2 per genotype. Differentially expressed genes (DEGs) were determined by the ones passing the threshold of adjusted p value 0.05 and the ABS (log2 Fold Change) 0.6 (for age-dependent transcriptome in Figures 1 and 2) or 0.3 (for experience-dependent transcriptome in Figures 5 and S7). Binomial

test with Bonferroni correction was used to determine over-represented GO-terms in the PANTHER Classification System (15.0, released 2020-07-28).

As for the hippocampal recording study, place cells recorded from 4 wildtype and 4 *Neil3*$^{-/-}$ mice were analyzed (Figures 3 and 4). Statistics was conducted using unpaired t-test with Welch's correction at the population level (each cell as statistical unit), but only reported as significant when passed a $p < 0.05$ in a nested t-test (pcorr., each animal as statistical unit, $n = 4$ for each genotype).

As for the IHC studies, all comparisons were conducted with 1 animal equaling 1 statistical unit (2-3 sections per animal) and 6 animals per genotype at different postnatal time points (Figure 1A) or at "Naive" and "SE" conditions (Figure 6). Whenever suitable, a two-way-ANOVA was used to compare results between groups, considering the factors *genotype and *intervention. A correction for multiple testing was performed in all cases, generally employing Sidak's method. Whenever only one variable differed between groups, a Student's t-test with Welch's correction was used.

All statistical analysis was conducted using GraphPad Prism Version 8 (GraphPad Software, San Diego, USA) and all statistic details were indicated in the figure legends as well as in the respective method sections.